14

2D Iterative Detection Network Based Image Restoration: Principles, Applications and Performance Analysis

Daniel Kekrt and Miloš Klíma
Dept. of Radio Engineering, Czech Technical University in Prague
Czech Republic

1. Introduction

Image capturing is corrupted by numerous perturbing influences. These influences are divisible to time-invariant and temporal. The typical time-invariant influence is an image blurring, rising from various causes, that can be mathematically understood as deterministic 2D ISI channel or FSM (Finite state machine). Among temporal influences pertain especially noises on the other hand. There are four significant noise sources in the case of a camera with CCD (CMOS) sensor: photon noise (signal dependent additive Poisson stochastic process), thermal noise (additive Poisson stochastic process), readout noise (additive Gaussian stochastic process) and quantization noise (J. van Vliet L. et al., 1998). The photon noise is caused by the time inhomogeneous photon emission, incident to the lens in individual par-axial light rays, with the mean value and squared standard deviation μ_P equal to the averaged intensity of these rays. The photon noise cannot be compensated because its origin is located front of the lens. Therefore we will not take it into account. The thermal noise, readout noise and quantization noise together create one composite noise of the CCD/CMOS sensor that affects on the captured blurred image as the random IECS-ML channel. Such channel is biased by three parameters μ_R, σ_R (mean value and standard deviation of the readout noise), depending on the sensor readout rate, and μ_T (mean value and squared standard deviation of the thermal noise), exponentially raising according to the sensor temperature T_s. All mentioned influences can be eliminated by iterative detection network (IDN). Such system solves effectively the 2D MAP criterion through feedback process based on the exchange and precision of certain probability density functions (PDFs). Similar networks (simpler one-dimensional alternatives) have found utilization in the sphere of Turbo code detection (Chugg et al., 2001; Vucetic & Juan, 2003; 2000). There will be discussed de facto theirs generalization to the two-dimensional form. The explanation begins by decomposition of the 2D MAP criterion that elucidates the essential principle of IDNs functioning. The necessary conditions for this decomposition will be defined too. Consequently, we focus closer to the IDNs dedicated for restoration of dichromatic images and using PDFs marginalization at the symbol level and symbol block level.

2. System model

We assume the model of image capturing system in Fig. 1 including three major sections. The first and second section are emulating all perturbing influences affecting the captured

image. The first section presents the hypothetical model of the time-invariant image blurring (2D ISI channel). The second one is image capturing section (IECS-ML channel) modeling all significant noises incident this kind of capturing systems. Such noises rise especially in the camera sensor with on-chip electronics, but no only there. The last section is the MAP criterion based iterative detector (restorative circuits) containing IDN with its front-end, so-called soft output demodulator (SODEM).

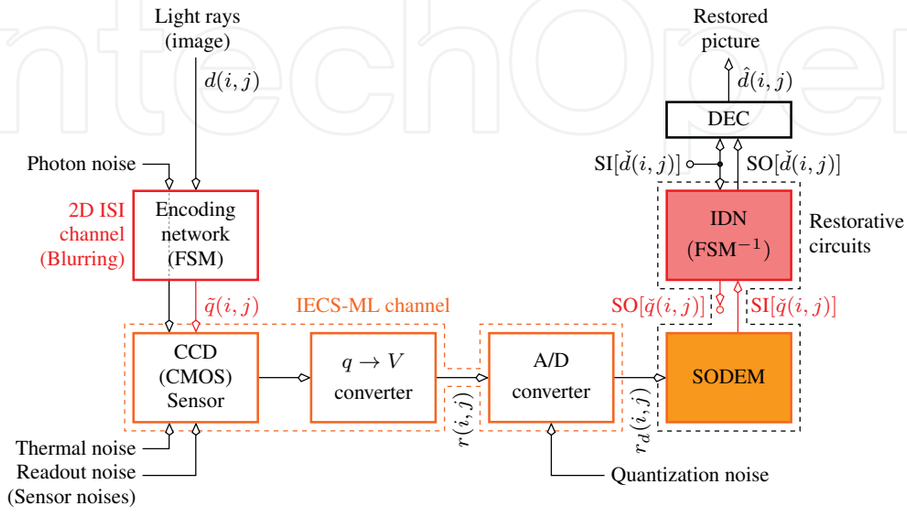

Fig. 1. Block diagram of a CCD/CMOS camera with dichromatic image restorative section.

3. Deterministic 2D ISI channel (blurring model)

A time-invariant image blurring can be emulated by the signal transmission through the 2D ISI channel defined via convolution

$$\begin{aligned}\tilde{q}(i,j) &= f(\mathbf{A}, \mathcal{N}_d(i,j) \subset \mathbf{D}) \\ &= \sum_{0 \le i',j' \le H_{\mathbf{A}},W_{\mathbf{A}}} a(i',j')d(i+i',j+j'),\end{aligned} \tag{1}$$

where $\mathcal{N}_d(i,j) = \{d(i+i',j+j')\}_{0 \le i',j' \le H_{\mathbf{A}},W_{\mathbf{A}}}$ denotes the convolution region and $\mathbf{D} = [d(i,j)]_{i,j}$ the page of black and white pixels $d(i,j) \in \{d^{(\ell)}\}_{\ell=1}^{M_d} = \{0,1\}$ (relative photon quantity impacting at the lens in several par-axial rays). The discrete 2D finite impulse response $\mathbf{A} = [a(i',j')]_{0 \le i',j' \le H_{\mathbf{A}},W_{\mathbf{A}}}$ with the high $H_{\mathbf{A}}$ and width $W_{\mathbf{A}}$ model time-invariant image blurring. There we focus closer to the two basic time-invariant distortion — defocusing in the imperfectly adjusted lens and blurring due to object moving.

3.1 Defocusing in the inperfectly adjusted lens

The image blurring in a defocused lens can be mathematically imitated as the Gaussian blurring channel (GBC). It is defined by the point spread function $PSF(x,y) = \frac{\Delta}{\pi} e^{-\Delta(x^2+y^2)}$, where Δ is the spread parameter. Two examples of $PSF(x,y)$ with different Δ shows Fig. 2.

If we want transform such PSF to the 2D ISI channel, we have to assume approximation, that the distribution of light is uniform on the flats with the size and shape congruous to the

sensor cells. Thereafter, the discrete convolution kernel can be got by the integration $a(i,j) = \int_{i-1/2}^{i+1/2}\int_{j-1/2}^{j+1/2} PSF(x,y)dxdy = \frac{\Delta}{4}(\mathrm{erf}(i-1/2)-\mathrm{erf}(i+1/2))(\mathrm{erf}(j-1/2)-\mathrm{erf}(j+1/2))$ of the $PSF(x,y)$ over the individual sensor cells. They are marked in Fig. 2 by the carnation lines and adjusted, without detriment to generality, as the unit size areas. Concretely, the results of the mentioned integration in our examples are two kernels

$$\mathbf{A}_{\mathrm{GBC},3/10} = \begin{bmatrix} 0.0458 & 0.1172 & 0.0458 \\ 0.1172 & 0.3000 & 0.1172 \\ 0.0458 & 0.1172 & 0.0458 \end{bmatrix}, \ \mathbf{A}_{\mathrm{SGBC},6/10} = \begin{bmatrix} 0 & 0.0872 & 0 \\ 0.0872 & 0.6000 & 0.0872 \\ 0 & 0.0872 & 0 \end{bmatrix}, \tag{2}$$

marked in the given figure by red stem graphs. The first is 9-ray kernel and the second one is 5-ray kernel with suppressed insignificant rays.

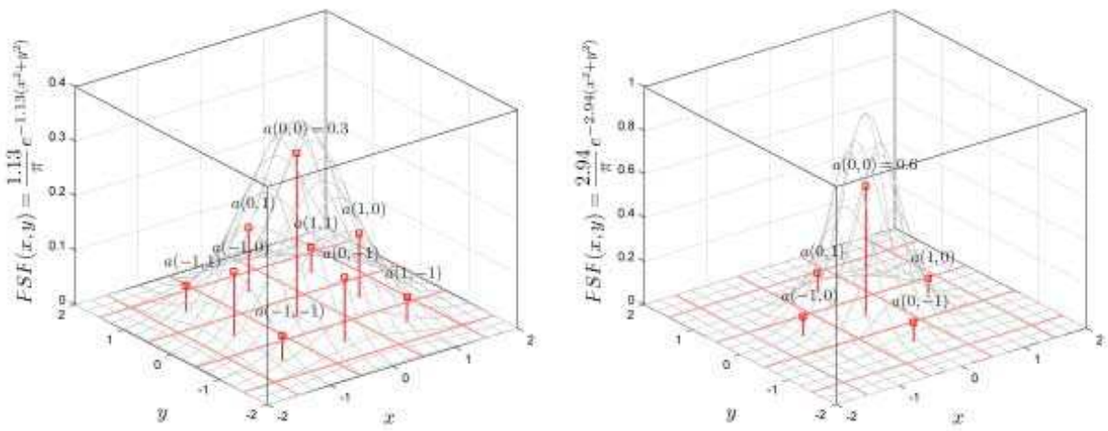

(a) $\mathbf{A}_{\mathrm{GBC},3/10}$. (b) $\mathbf{A}_{\mathrm{SGBC},6/10}$.

Fig. 2. The two examples of GBCs with corresponding convolutional kernels.

$a(0,0) = 0.2$ $a(0,0) = 0.3$ $a(0,0) = 0.4$ $a(0,0) = 0.5$ $a(0,0) = 0.7$ $a(0,0) = 1$

Fig. 3. Examples of the defocusing by GBC on the QR code snapshot.

3.2 Blurring due to object moving

We have an object moving on the certain known trajectory as well as in Fig. 4. Each point of this object pass the curve $\mathbf{s}(t') = [s_x(t')\ s_y(t')]$ with the starting $\mathbf{s}_s = \mathbf{s}(t)$ and ending $\mathbf{s}_e = \mathbf{s}(t+T_e)$ point. These points are projected through the lens (it is not included to Fig. 4 for simplicity) to the plane $\{\mathbf{b}_x, \mathbf{b}_y\}$ of the CCD/CMOS sensor, where T_e is the exposure time. We denote impulse response of the channel emulating blurring due to object moving as $\mathbf{A}_{\mathrm{BOM},\alpha}$ and with respect to discrete character of this response let us approximate the

realization of par-axial intensity on the plane $\{\mathbf{b}_x, \mathbf{b}_y\}$, in the time t, as the mosaic $D(x,y) = \sum_{i,j} d(i,j) f_p(i,j,x,y)$ of pixels $d(i,j) \in \{d^{(\ell)}\}_{\ell=1}^{M_d}$ shaped by square function

$$f_p(i,j,x,y) = \begin{cases} 1 \text{ iff } |x - iL_p| \leq \frac{L_p}{2} \wedge |y - jL_p| \leq \frac{L_p}{2} \\ 0 \qquad\qquad \text{otherwise} \end{cases}, \tag{3}$$

where L_p establish their size, that is equal or less then size L_c of the sensor cell (potential well).

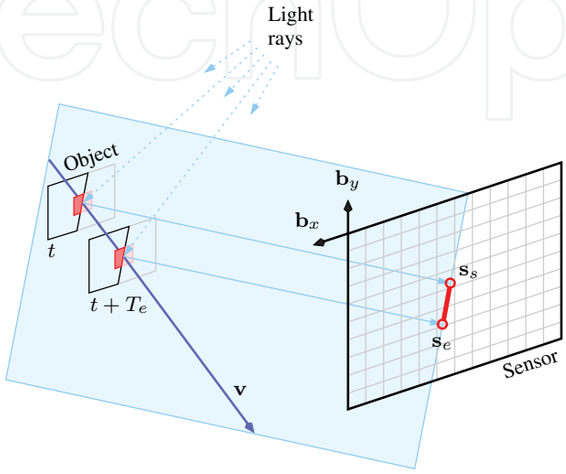

Fig. 4. The projection of the moving object point to the CCD/CMOS sensor plane.

On the basis of declared definitions and approximations, we can subsequently express useful signal impacting the sensor by the convolution Eq. 1 emulating the situation, when the snapshot $\mathbf{D}$, gained in the time t, is slided on the sensor surface and stepwise trapped to the its cells. The said fact can be also conceived from the opposite side, when potential well sliding on the immovable pattern $\mathbf{D}$. If the velocity radial component is insignificant in the comparison with axial component (expansion of the object is negligible between times t and $t + T_e$) and starting time t is equated to zero, we can obtain the impulse response coefficients by the integration

$$a(i',j') \propto \int_0^{T_e} \int_{s_y(t')-\frac{1}{2}L_p}^{s_y(t')+\frac{1}{2}L_p} \int_{s_x(t')-\frac{1}{2}L_p}^{s_x(t')+\frac{1}{2}L_p} f_p(i(\mathbf{s}_s)+i', j(\mathbf{s}_s)+j', x', y') dx' dy' dt'. \tag{4}$$

This situation illustrate Fig. 5a or Fig. 5b. The responses

$$\mathbf{A}_{\mathrm{BOM},0} = \left[\, \tfrac{1}{12} \;\; \tfrac{1}{6} \;\; \tfrac{1}{6} \;\; \tfrac{1}{6} \;\; \tfrac{1}{6} \;\; \tfrac{1}{6} \;\; \tfrac{1}{6} \;\; \tfrac{1}{12} \,\right]^T, \; \mathbf{A}_{\mathrm{BOM},\pi/4} = \begin{bmatrix} \frac{1}{6} & \frac{1}{12} & 0 \\ \frac{1}{12} & \frac{1}{3} & \frac{1}{12} \\ 0 & \frac{1}{12} & \frac{1}{6} \end{bmatrix} \tag{5}$$

can be stated as the examples of such distortion channels that come from Eq. 4 biased by angles $\varphi = 0$, $\varphi = \frac{\pi}{4}$ and with confinement only to equable movement, when $\mathbf{s}(t')$ is linear function of time t'.

If the object expansion on the plane $\{\mathbf{b}_x, \mathbf{b}_y\}$, between the times t and $t + T_e$, is not insignificant the situation in Fig. 5c occurs. Computation of the constants

$$a(i', j') \propto \int_0^{T_e} \int_{s_y(t')-\frac{1}{2}L_c(t')}^{s_y(t')+\frac{1}{2}L_c(t')} \int_{s_x(t')-\frac{1}{2}L_c(t')}^{s_x(t')+\frac{1}{2}L_c(t')} f_p(i(\mathbf{s}_S)+i', j(\mathbf{s}_S)+j', x', y')dx'dy'dt' \qquad (6)$$

is analogical to Eq. 4, only with the difference that size of sliding sensor cell will not be equal to pixel size L_p anymore, but it will present the function $L_c(t')$ linearly (Fig. 5c) or non-linearly dependent on the time t' in compliance with the movement of scanning object.

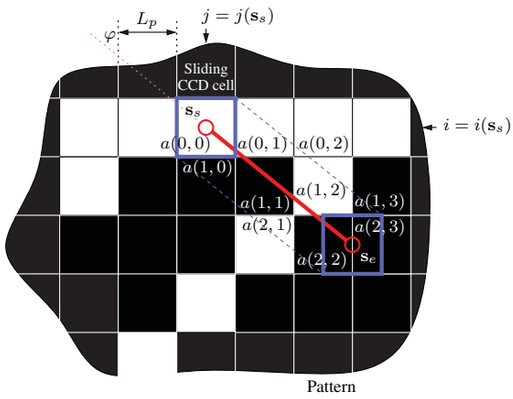

(a) The example with $\mathbf{s}_S$ situated inside of the pixel $(i(\mathbf{s}_S), j(\mathbf{s}_S))$. Negligible radial component of the velocity.

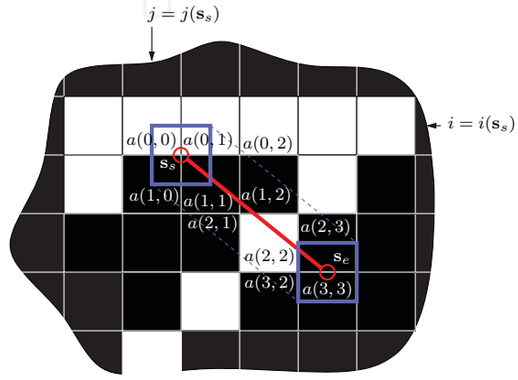

(b) The example with $\mathbf{s}_S$ situated on the edge of the pixel $(i(\mathbf{s}_S), j(\mathbf{s}_S))$. Negligible radial component of the velocity.

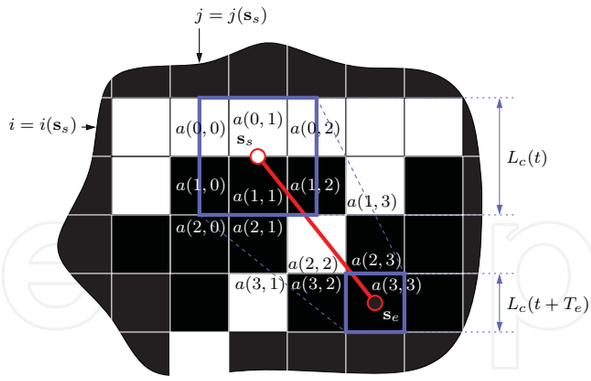

(c) The example with $\mathbf{s}_S$ situated on the edge of the pixel $(i(\mathbf{s}_S), j(\mathbf{s}_S))$. Indispensable radial component of the velocity.

Fig. 5. The equivalent movement trajectory of the sensor sensing cell sliding on the pattern **D** (snapshot of the straight-line moving object with negligible and indispensable radial component of the velocity **v**).

3.3 Hypothetical cellular model of a 2D ISI channel — Encoding network (EN)

The convolution Eq. 1 can be emulated by certain 2D hypothetical encoding network (EN). The assembly of this EN is variable and contains specific, relatively simple, functional blocks $f_G()$. We denote these functional blocks as general processing elements (GPEs) and one such elements is illustrated in Fig. 6a.

In principle, a GPE presents a simple FSM whose inputs as well as outputs are variables $\mathcal{S}(k)$ discrete in values, that are derivable from alphabets $\{\mathcal{S}^{(\ell)}(k)\}_\ell$. The inputs together with the outputs consequently create the set $\mathcal{N} = \bigcup_k \mathcal{S}(k)$ flowing from the alphabet $\{\mathcal{N}^{(\ell)}\}_\ell$.

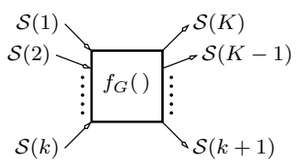

(a) A GPE.

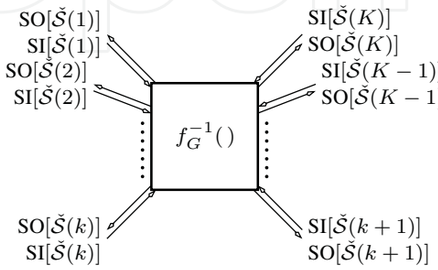

(b) A SISO module.

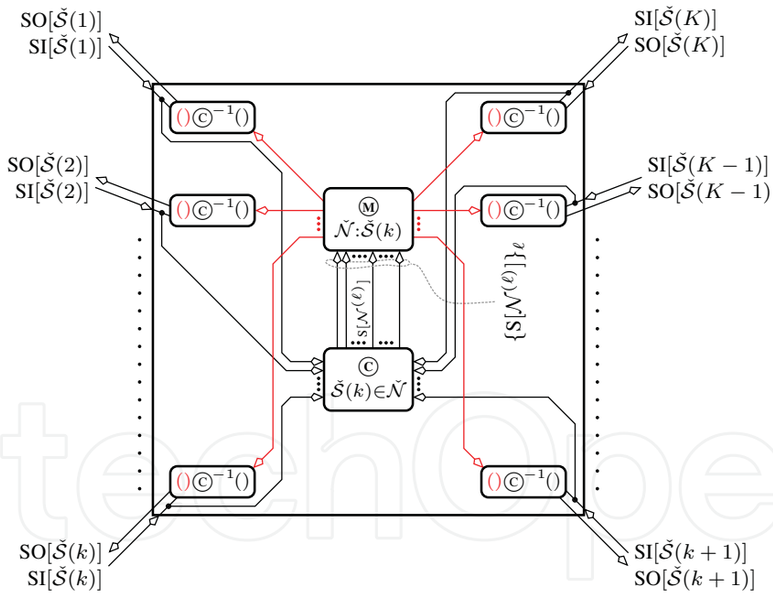

(c) Structure of a SISO module.

Fig. 6. A general processing element (GPE) and its soft inversion (SISO module).

4. Random IECS-ML channel (noise model)

4.1 Composite noise of the CCD/CMOS sensor

The presence of the signal independent composite CCD/CMOS sensor noise in mutually correlated rays $0 \leq \tilde{q}(i,j) \leq 1$ can be expressed as the blurred image transmission through

the random IECS-ML channel with I/O equation $r(i,j) = C\tilde{q}(i,j) + w_T(i,j) + w_R(i,j)$, where $r(i,j)$ is the channel output, $w_T(i,j)$ is the total thermal noise accumulated with the useful signal $q(i,j) = C\tilde{q}(i,j)$ as a charge in the CCD sensor cell at the position (i,j) and $w_R(i,j)$ is the readout noise. The constant C (above limited by a full well capacity FWC of the CCD sensor) defines a quantity of generated charge and it is directly proportional to the exposure time T_e.

4.2 Quantization noise of the A/D converter

The output $r(i,j)$ (IECS-ML channel output also registrable in the matrix form $\mathbf{R} = \mathbf{Q} + \mathbf{W}_T + \mathbf{W}_R$ for entire sensor) is further quantized in the N_b-bit A/D converter that can be approximated by the random channel $r_d(i,j) = r(i,j) + w_Q(i,j)$ with uniformly distributed noise $w_Q(i,j)$ in light of probability theory. We denote the output of this converter as $r_d(i,j) = Q(r(i,j))$, where $Q(\xi) = \sum_{1 \le \ell \le 2^{N_b}} H(\xi - t_Q(\ell))$ and $H(\xi) = \{ {0 \atop 1} {\text{iff} \atop \text{otherwise}} {\xi < 0 \atop } \}$ is a Heaviside step function. For simplicity we will assume the linear quantization only with threshold values

$$t_Q(\ell) = \begin{cases} 0 & \text{iff} \quad \ell = 1 \\ (\ell - 1)\Delta_Q + 1/2 & \text{iff} \ \ 1 < \ell \le 2^{N_b} \end{cases} \tag{7}$$

and quantization step Δ_Q, where for the highest quantization level $t_Q(2^{N_b}) \le FWC$ is applied.

5. Image restoration — Symbol and page 2D MAP detection

5.1 Optimal MAP detection

The channel has independent eliminated states (IECS), if noise sources in CCD sensor cells are mutually independent. It makes joint probability density function (PDF) $p_{\mathbf{W}}(\Xi) = \prod_{i,j} p_w(\xi)$ as the product of marginal densities. The channel is memory-less (ML), if the current $x(i,j)$ depends only on the corresponding $q(i,j)$. The fulfillment of both conditions creates the likeli-hood function

$$\begin{aligned} p_{\mathbf{R}}(\Xi|\check{\mathbf{Q}}) &= \int_{\mathbf{W}} p_{\mathbf{R}|\mathbf{Q},\mathbf{W}}(\Xi|\check{\mathbf{Q}}, \Xi') p_{\mathbf{W}}(\Xi') d\Xi' \\ &= \prod_{i,j} \underbrace{\int_{w(i,j)} p_{r|q,w}(\xi|\check{q}(i,j), \xi') p_w(\xi') d\xi'}_{p_r(\xi|\check{q}(i,j))} \end{aligned} \tag{8}$$

factorizable that is necessary to transition from a single-stage detector to an IDN.

The optimal 2D MAP detector is based on the criterion

$$\hat{d}(i,j) = \arg \underset{\check{d}(i,j)}{\text{Ⓜ}} \left[\underset{\check{\mathbf{D}}:\check{d}(i,j)}{\text{Ⓜ}} \mathrm{S}[\mathbf{R}_d, \check{\mathbf{D}}] \right], \tag{9}$$

where $\hat{d}(i,j)$ denotes the wanted estimation, $\check{d}(i,j)$ denotes a testing estimator (takes individual values from data alphabet), $\check{\mathbf{D}} : \check{d}(i,j)$ denotes the set of possible image realizations containing the estimator $\check{d}(i,j)$ and Ⓜ with Ⓜ denote certain types of marginalization operators.

The quantity $\mathrm{S}[\mathbf{R}_d, \check{\mathbf{D}}]$ is to be understood as some kind of the joint soft measure and due to IECS-ML condition fulfillment

$$\begin{aligned}\mathrm{S}[\mathbf{R}_d|\check{\mathbf{D}}] &= \underset{i,j}{\copyright}\mathrm{S}[r_d(i,j)|\check{\mathbf{D}}] \\ &= \underset{i,j}{\copyright}\mathrm{S}[r_d(i,j)|\check{\mathcal{N}}_d(i,j) \subset \check{\mathbf{D}}] \end{aligned} \tag{10}$$

with assumption of a statistically independent data $\mathrm{S}[\check{\mathbf{D}}] = \underset{i,j}{\copyright}\mathrm{S}[\check{d}(i,j)]$ can be decomposed to the form

$$\begin{aligned}\mathrm{S}[\mathbf{R}_d, \check{\mathbf{D}}] &= \mathrm{S}[\mathbf{R}_d|\check{\mathbf{D}}]\copyright\mathrm{S}[\check{\mathbf{D}}] \\ &= \left(\underset{i,j}{\copyright}\mathrm{S}[r_d(i,j)|\check{\mathcal{N}}_d(i,j) \subset \check{\mathbf{D}}]\right) \copyright \left(\underset{i,j}{\copyright}\mathrm{S}[\check{d}(i,j)]\right) \end{aligned} \tag{11}$$

that is joined by certain types of combination operators ($\copyright$, $\copyright$). On the basis of marginalization and combination operators, we can split detectors into four groups in light of detection technique (symbol or page) and implementing domain (probability $\mathrm{P}[\,]$ or equivalent logarithmic metric $\mathrm{M}[\,] = -\ln(\mathrm{P}[\,])$). All possibilities are summarized in Table 1.

The symbol technique (SyD) seeks to minimize of the actual symbol detection error only. The page detection (PgD) has tendency to minimization the entire page detection error. The most numerically effective is the Md-PgD alternative, because it contains the simple combination operator as well as the simple marginalization operator. Close to the Md-PgD, the Md-SyD conjunction with the relatively simple marginalization operator $\min^*(x,y) = \min(x,y) - \ln(1+e^{-|x-y|})$.

Domain	S[ ]	Detection	Ⓜ	Ⓜ	©	©	$\copyright^{-1}$
Probability (Pd)	P[ ]	Page (PgD)	max	max	Π	$\times$	$\div$
Probability (Pd)	P[ ]	Symbol (SyD)	max	Σ	Π	$\times$	$\div$
Metric (Md)	M[ ]	Page (PgD)	min	min	Σ	+	$-$
Metric (Md)	M[ ]	Symbol (SyD)	min	$\min^*$	Σ	+	$-$

Table 1. Summary of combination and marginalization operators.

5.2 Suboptimal MAP detection

The direct evaluation of the $\hat{\mathbf{D}}$ from the criterion (9) (single-stage detection) is impossible, because it requires a sequent substitution of all potential image realizations $\check{\mathbf{D}}$. But Eq. 10 (IECS-ML condition) makes possible decomposition of the detection problem from the entire page $\mathbf{D}$ to the level of individual (mutually overlapping) convolution regions $\mathcal{N}_d(i,j)$, corresponding to individual captured pixels. Therefore, we can substitute the single-stage MAP detector by the sub-optimal iterative detection network (IDN).

Such network is formed from a definite number of functional blocks, so-called soft inversions (SISO modules), that exchange the soft measures with each other. The SISO modules present statistical devices complementary to the GPEs in the appropriately designed hypothetical EN

emulating the image blurring. The fulfillment of the condition IECS-ML enables a usage of such GPEs that compose the hypothetical realization $\check{\mathbf{D}}$ of a sensing image even by smallest parts (by individual pixels $\check{d}(i,j)$) if this yields a implementation benefits in light of concrete modeled distortion.

The IDN output can be regarded as a optimal (identical with the output of single-stage detector) after the execution of infinite number of iterations (information interchange between inversions). It is not practicable. Therefore, the IDN with the finite number of iterations is sub-optimal detector, that generally provides an inferior estimation to the single-stage detector. Roughly speaking the IDN contains simpler SISO modules, the IDN is more numerically effective and more sub-optimal (it includes more iteratively refining variables).

In the course of each iteration I of the IDN, from count N_I, is every SISO module once activated at the least. The activation rests in the reading of soft measures (whole probability or metric densities $\{\mathrm{SI}[\mathcal{S}^{(\ell)}(k)]\}_\ell$, corresponding to certain random variable $\mathcal{S}(k)$ in the hypothetical model) on inputs of a SISO module, followed by the enumeration of output soft measures (whole densities $\{\mathrm{SO}[\mathcal{S}^{(\ell)}(k)]\}_\ell$). The current iteration concludes the exchange of soft measures

$$\begin{aligned} \{\mathrm{SO}[\mathcal{S}^{(\ell)}(k)]\}_\ell &\rightarrow \{\mathrm{SI}[\mathcal{S}^{(\ell)}(k)]\}_\ell \\ \{\mathrm{SI}[\mathcal{S}^{(\ell)}(k)]\}_\ell &\leftarrow \{\mathrm{SO}[\mathcal{S}^{(\ell)}(k)]\}_\ell \end{aligned} \tag{12}$$

among the neighboring modules. After execution of all iteration N_I, the estimations of all wanted (output) random variables are performed from the formula

$$\hat{\mathcal{S}}(k) = \arg \underset{\check{\mathcal{S}}(k)}{\text{Ⓜ}} [\mathrm{SI}[\check{\mathcal{S}}(k)] \text{Ⓒ} \mathrm{SO}[\check{\mathcal{S}}(k)]]. \tag{13}$$

We express this operation as a hard decision provided by a decision block (DEC).

6. Iterative detection networks

6.1 IDN topology and soft inversion $f_G^{-1}()$ (SISO module) of general processing element $f_G()$ (FSM)

An IDN presents a soft inversion of an arbitrary EN formed from certain mutually concatenated GPEs that jointly execute an arbitrary processing with input signal. In the our case, as was said in the paragraph 3.3, such EN executes the convolution Eq. 1 and due to fulfillment of the IECS-ML condition can contain the simplest GPEs working on the level of individual pixels. The IDN topology exactly agrees to the EN topology only with the difference, that each of GPE is substituted by its SISO module, just like in Fig. 6a, 6b. The signal processing in the soft inversion is implied in Fig. 6c and takes place in two steps. Firstly, the inputs $\{\mathrm{SI}[\mathcal{S}^{(\ell)}(k)]\}_{\ell,k}$ are combined to particular joint soft measures

$$\mathrm{S}[\check{\mathcal{N}}] = \underset{\check{\mathcal{S}}(k)\in\check{\mathcal{N}}}{\text{Ⓒ}} \mathrm{SI}[\check{\mathcal{S}}(k)] \;\text{ for }\; \forall\check{\mathcal{N}}. \tag{14}$$

Consequently, all joint measures $\{\mathrm{S}[\mathcal{N}^{(\ell)}]\}_\ell$, corresponding to the set $\forall\check{\mathcal{N}}$ of possible realizations $\mathcal{N}^{(\ell)}$, are marginalized to outputs $\{\mathrm{SO}[\mathcal{S}^{(\ell)}(k)]\}_{\ell,k}$

$$\mathrm{SO}[\check{\mathcal{S}}(k)] = \left(\underset{\check{\mathcal{N}}:\check{\mathcal{S}}(k)}{\text{Ⓜ}} \mathrm{S}[\check{\mathcal{N}}] \right) \text{Ⓒ}^{-1} \mathrm{SI}[\check{\mathcal{S}}(k)] \;\text{ for }\; \forall\check{\mathcal{S}}(k) \tag{15}$$

that are connected to the inputs $\{\mathrm{SI}[\mathcal{S}^{(\ell)}(k)]\}_{\ell,k}$ of neighboring soft inversions. This update of soft information is known as a soft inversion activation. The activation accomplishment of all soft inversions in the IDN afterwards makes one iteration of the IDN.

6.2 Soft-output demodulator

The IDN closely cooperates with the SODEM (Soft output demodulator) providing fundamental hypothesis about captured signal $\mathbf{R}_d$. This functional block presents a gateway between the domain of a real realizations (realizations of certain random variables), where are operated with scalars (factual realizations), and the probability (metric) domain of the IDN, where are operated with whole densities. The SODEM includes the likeli-hood function (or transfer function) of the IECS-ML channel emulating all noises incident in the image capturing system chain (in the our case it is CCD/CMOS camera). The SODEM input forms realization $r_d(i,j)$ that is inside transformed to the discrete a posteriori density $\{\mathrm{SI}[q^{(\ell)}(i,j)]\}_\ell$ presenting the input (sufficient statistic) of the IDN.

Before the sufficient statistic derivation as such, it should be noted that the derivation is purely theoretical and does not correspond to any particular type of CCD / CMOS sensor. We start the SODEM derivation with the definition of discrete cut off Gaussian PDF

$$\begin{aligned} p_{\mathcal{N}_0^{\mathrm{FWC}}}(\xi,\mu,\sigma) \approx & \frac{1}{\sqrt{2\pi}\sigma}\sum_{\ell=0}^{\mathrm{FWC}}\delta(\xi-\ell)\exp\left(-\frac{(\ell-\mu)^2}{2\sigma^2}\right) \\ & +\frac{1}{2}\delta(\xi-\mathrm{FWC})\mathrm{erfc}\left(\frac{2\mathrm{FWC}+1-2\mu}{\sqrt{8}\sigma}\right) \\ & +\delta(\xi)\left(1-\frac{1}{2}\mathrm{erfc}\left(-\frac{1+2\mu}{\sqrt{8}\sigma}\right)\right). \end{aligned} \tag{16}$$

All parameters FWC, ξ, μ, σ, etc. in all densities, we will assume in terms of number of electrons [-] either directly or as equivalent quantities related to number of electrons (for example: the quantization noise occurring in the A/D converter, we will consider as if the equivalent electron noise source deteriorative in the sensor, etc.). On the basis of the mentioned definition can be formed thermal and readout noise PDFs as

$$p_{w_T}(\xi) \approx \begin{cases} 0 & \text{iff } \begin{smallmatrix}\mu_T<40\\ \xi\geq 70\end{smallmatrix} \\ e^{-\mu_T}\sum_{\ell\in\mathbb{N}_0}\frac{\mu_T^\ell}{\ell!}\delta(\xi-\ell) & \text{iff } \begin{smallmatrix}\mu_T<40\\ \xi<70\end{smallmatrix} \\ p_{\mathcal{N}_0^{\mathrm{FWC}}}(\xi,\mu_T,\sqrt{\mu_T}) & \text{iff } \mu_T\geq 40 \end{cases} \tag{17}$$

and

$$p_{w_R}(\xi) = p_{\mathcal{N}_0^{\mathrm{FWC}}}(\xi,\mu_R,\sigma_R). \tag{18}$$

Both noises together then create the composite noise $w(i,j) = w_T(i,j) + w_R(i,j)$ and examples of theirs densities, for certain parameters μ_T, μ_R and σ_R, is shown in Fig. 7.

The mentioned PDFs are biased by three parameters μ_R, σ_R and μ_T. First two parameters are known, because depend on the sensor readout rate that is also known. The last one is the nuisance unknown parameter consisting in the unknown CCD/CMOS sensor temperature and has to be estimated by a suitable way. A ML estimation $\hat{\mu} = N^{-1}\sum_{k=1}^{K} w(k)$ can be used

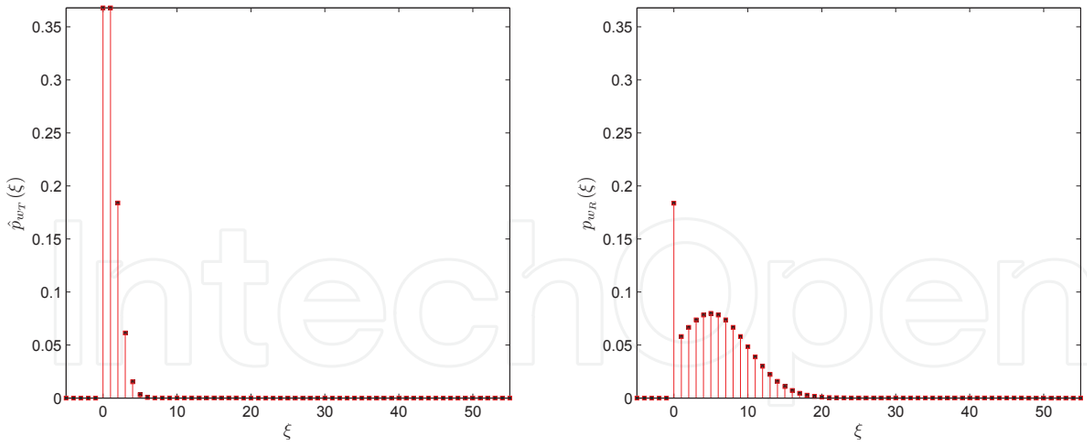

Fig. 7. The example of the thermal and readout noise PDF for $\mu_T = 1$, $\mu_R = 5$, $\sigma_R = 5$ and FWC $= 50$.

for such purpose, which represents the solution of the equation

$$\frac{d}{d\mu} \sum_{k=1}^{K} \ln \left(e^{-\mu} \frac{\mu^{w(k)}}{w(k)!} \right) \Bigg|_{\mu=\hat{\mu}} = 0 \tag{19}$$

derived from the ML criterion. The set of values $\{w(1), w(2), \ldots, w(k), \ldots, w(K)\}$ is the realization of the composite noise on the blacked out CCD sensor strip. The average value of the composite noise $\hat{\mu}$, obtained by the measurement from the blacked out area is used for the computation of $\hat{\mu}_T = \hat{\mu} - \mu_R$. That, substituted back to the density $p_{w_T}(\xi)$, produces its estimation $\hat{p}_{w_T}(\xi)$.

Statistical properties of the composite noise $w(i,j)$ presents the wanted noise model, that controls the IECS-ML channel (channel with additive noise) behavior and results from the

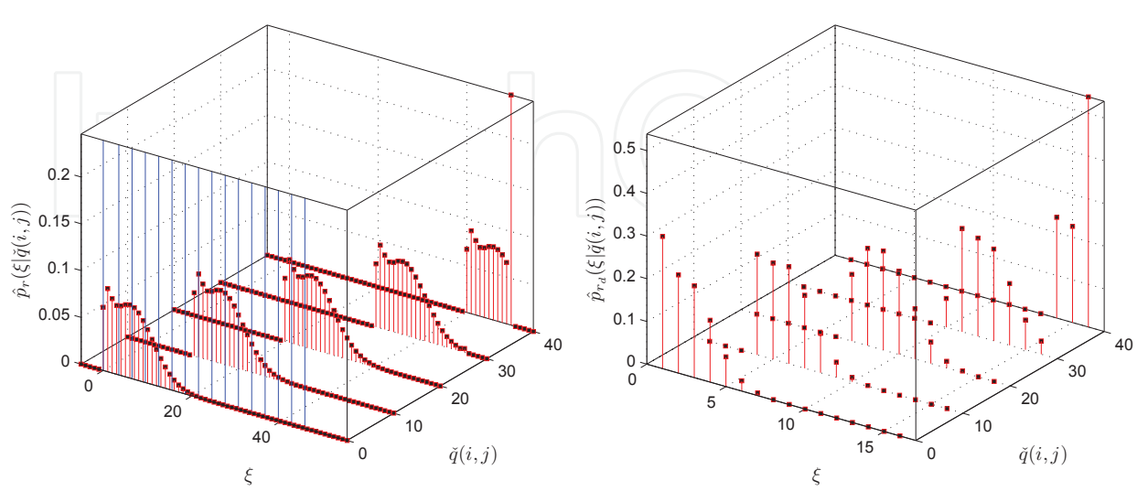

Fig. 8. The $\hat{p}_r(\xi|\breve{q}(i,j))$ and $\hat{p}_{r_d}(\xi|\breve{q}(i,j))$ PDF corresponding to the given examples densities of the thermal and readout noise. $N_b = 4$ and $\Delta_Q = 3$.

cut off PDF

$$\hat{p}_w(\xi) \approx \hat{p}'_w(\xi) + \delta(\xi - \mathrm{FWC}) \left(1 - \int_{-\frac{1}{2}}^{\mathrm{FWC}+\frac{1}{2}} \hat{p}'_w(\xi')d\xi'\right), \tag{20}$$

based on the convolution

$$\hat{p}'_w(\xi) = \sum_{\ell=0}^{\mathrm{FWC}} \delta(\xi - \ell) \int_{-\frac{1}{2}}^{\xi+\frac{1}{2}} \hat{p}_{w_T}(\ell - \xi') p_{w_R}(\xi')d\xi' \tag{21}$$

of densities $\hat{p}_{w_T}(\xi)$ and $p_{w_T}(\xi)$.

The procedure obtaining the metric $\mathrm{SI}[\check{q}(i,j)]$ from the derived noise model begins with the elimination Eq. 10 of the noise density $\hat{p}_w(\xi)$ out of the likeli-hood function of a channel with additive noise $p_{\mathbf{R}|\mathbf{Q},\mathbf{W}}(\Xi|\check{\mathbf{Q}},\Xi') = \delta(\Xi - (\check{\mathbf{Q}} + \Xi'))$ or $p_{r|q,w}(\xi|\check{q}(i,j),\xi') = \delta(\xi - (\check{q}(i,j) + \xi'))$, assuming perfect knowledge of the noise realization $\mathbf{W}$. The result of this elimination is the density $\hat{p}_r(\xi|\check{q}(i,j)) = \hat{p}_w(\check{q}(i,j) - \xi)$. Along with the thermal noise, another source of noise is found in the chain. It is the quantization noise with the uniform PDF p_{w_Q} which is added to the signal in the A/D converter. It can be eliminated out of the density $\hat{p}_r$ by the integrating

$$\begin{aligned}\hat{p}_{r_d}(\xi|\check{q}(i,j)) = {} & \delta(\xi - 2^{N_b}) \lim_{\epsilon\to 0^+} \int_{t_Q(2^{N_b})-\epsilon}^{\mathrm{FWC}+\frac{1}{2}} \hat{p}_r(\xi'|\check{q}(i,j))d\xi' \\ & + \sum_{\ell=1}^{2^{N_b}-1} \delta(\xi - \ell) \lim_{\epsilon\to 0^+} \int_{t_Q(\ell)-\epsilon}^{t_Q(\ell+1)-\epsilon} \hat{p}_r(\xi'|\check{q}(i,j))d\xi'\end{aligned} \tag{22}$$

over individual quantization steps (by averaging with the density p_{w_Q}) of the size Δ_Q expressed in the number of electrons and defined, in our case, by Eq. 7. In Fig. 8 you can see the examples of the densities $\hat{p}_r(\xi|\check{q}(i,j))$ and $\hat{p}_{r_d}(\xi|\check{q}(i,j))$ coming out of the given demonstrations in Fig. 7 if and only if $\check{q}(i,j) \in \{q^{(\ell)}\}_{\ell=1}^{M_q} = \{0, 10, 20, 30, 40\}$. We would like to emphasize that it is just a simple example and actually the cardinality of set $\{q^{(\ell)}\}_{\ell=1}^{M_q} = f(\mathbf{A}, \{\mathcal{N}_d(i,j)\}_{\ell=1}^{M_{\mathcal{N}_d}})$ is much larger then 5. Blue lines on Fig. 8 represent boundaries of the individual quantization steps.

The SODEM output can be obtained from the derived density by the integration

$$\mathrm{PI}[\check{q}(i,j)] = \int_{r_d(i,j)-\frac{1}{2}}^{r_d(i,j)+\frac{1}{2}} \hat{p}_{r_d}(\xi'|\check{q}(i,j))d\xi'. \tag{23}$$

On the following Fig. 9a, 9c, 9e, 9g are introduced four examples of the SODEM transfer function constituting the derived composite CCD/CMOS noise model for the blurring channel $\mathbf{A}_{\mathrm{GBC},3/10}$ (Eq. 2) and $\mathbf{A}_{\mathrm{BOM},\pi/4}$ (Eq. 5). For the purpose of higher lucidity was chosen continuous plotting, although the transfer functions have a discrete domain of definition. The individual demonstrations of transfer functions afterwards construe with samples (realizations) of captured images on Fig. 9b, 9d, 9f, 9h.

7. Distributed iterative detection networks

7.1 Distributed IDN marginalizing at the symbol block level

Firstly we focus on the IDNs marginalizing at the symbol block level with horizontal and vertical state variable. These IDNs result from the EN [1] in Fig. 10a where each node (GPE), shown in Fig. 11b, creates a one functional block with the fixed system of inputs and outputs $\mathcal{N}_f(i,j) = \{\mathcal{R}(i,j), \mathcal{C}(i,j), d(i+H_{\mathbf{A}}, j+W_{\mathbf{A}}), \mathcal{R}(i,j+1), \mathcal{C}(i+1,j), q(i,j)\}$, where $\mathcal{R}(i,j)$ and $\mathcal{C}(i,j)$ present auxiliary state variables containing more symbols together. Shapes of these variables are established by the condition

$$\begin{aligned}\mathcal{N}_d(i,j) \subseteq\ & \mathcal{R}(i,j) \cup \mathcal{C}(i,j) \cup d(i+H_{\mathbf{A}}, j+W_{\mathbf{A}}) \\ \supset\ & \mathcal{R}(i,j+1), \mathcal{C}(i+1,j).\end{aligned} \tag{24}$$

The optimal decomposition of the convolution region is $\mathcal{N}_d(i,j) = \mathcal{R}(i,j) \cup \mathcal{C}(i,j) \cup d(i+H_{\mathbf{A}}, j+W_{\mathbf{A}})$ and it is possible when $a(H_{\mathbf{A}}, W_{\mathbf{A}}) \neq 0$.

In the case of a channel $\mathbf{A}_{\mathrm{GBC},a(0,0)}$, with regard to the condition Eq. 24, the variables are $\mathcal{R}(i,j) = \{d(i,j), d(i,j+1), d(i+1,j), d(i+1,j+1), d(i+2,j), d(i+2,j+1)\}$ and $\mathcal{C}(i,j) = \{d(i,j), d(i,j+1), d(i,j+2), d(i+1,j), d(i+1,j+1), d(i+1,j+2)\}$. Their shapes you can see in Fig. 12a. In a similar way we can get decomposition of the $\mathcal{N}_d(i,j)$ for a channel $\mathbf{A}_{\mathrm{GBC},a(0,0)}$. One of possible results is shown in Fig. 12b.

The IDN has same topology as the EN and each its node forms SISO module, illustrated in Fig. 11b, performing the combination

$$\begin{aligned}\mathrm{S}[\check{\mathcal{N}}_f(i,j)] = \mathrm{SI}[\check{\mathcal{R}}(i,j)] \copyright \mathrm{SI}[\check{\mathcal{C}}(i,j)] \copyright \mathrm{SI}[\check{d}(i+H_{\mathbf{A}}, j+W_{\mathbf{A}})] \copyright \mathrm{SI}[\check{\mathcal{R}}(i,j+1)] \\ \copyright \mathrm{SI}[\check{\mathcal{C}}(i+1,j)] \copyright \mathrm{SI}[\check{q}(i,j)]\end{aligned} \tag{25}$$

with marginalizations

$$\mathrm{SO}[\check{\mathcal{R}}(i,j+j')] = \left(\mathop{\circledM}_{\check{\mathcal{N}}_f(i,j):\check{\mathcal{R}}(i,j+j')} \mathrm{S}[\check{\mathcal{N}}_{f()}(i,j)] \right) \copyright^{-1} \mathrm{SI}[\check{\mathcal{R}}(i,j+j')] \ \text{ for } \ j' \in \{0,1\}, \tag{26}$$

$$\mathrm{SO}[\check{\mathcal{C}}(i+i',j)] = \left(\mathop{\circledM}_{\check{\mathcal{N}}_f(i,j):\check{\mathcal{C}}(i+i',j)} \mathrm{S}[\check{\mathcal{N}}_{f()}(i,j)] \right) \copyright^{-1} \mathrm{SI}[\check{\mathcal{C}}(i+i',j)] \ \text{ for } \ i' \in \{0,1\}, \tag{27}$$

$$\mathrm{SO}[\check{d}(i+H_{\mathbf{A}}, j+W_{\mathbf{A}})] = \left(\mathop{\circledM}_{\check{\mathcal{N}}_f(i,j):\check{d}(i+H_{\mathbf{A}},j+W_{\mathbf{A}})} \mathrm{S}[\check{\mathcal{N}}_{f()}(i,j)] \right) \copyright^{-1} \mathrm{SI}[\check{d}(i+H_{\mathbf{A}}, j+W_{\mathbf{A}})], \tag{28}$$

and

$$\mathrm{SO}[\check{q}(i,j)] = \left(\mathop{\circledM}_{\check{\mathcal{N}}_f(i,j):\check{q}(i,j)} \mathrm{S}[\check{\mathcal{N}}_{f()}(i,j)] \right) \copyright^{-1} \mathrm{SI}[\check{q}(i,j)]. \tag{29}$$

One iteration of such IDN rests in the serial activation of each SISO module from the upper left corner to the lower right corner in the IDN as is marked by the light blue curve in Fig. 10a. After finishing all iterations, of the chosen count N_I, the IDN makes hard decisions $\hat{d}(i,j)$ per Eq. 13.

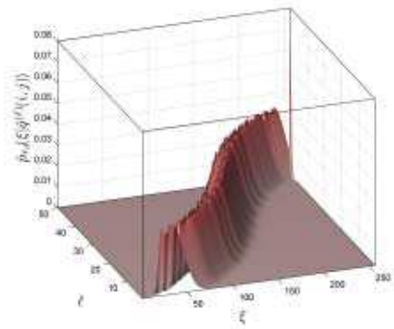

(a) The PDF for the blurring channel $\mathbf{A}_{\mathrm{GBC},3/10}$: $C = 612$, $\mu_T = 60$, $\mu_R = 40$, $\sigma_R = 35$.

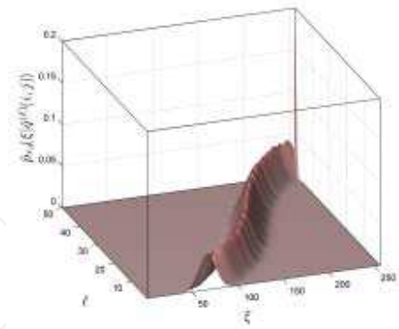

(b) The PDF for the blurring channel $\mathbf{A}_{\mathrm{GBC},3/10}$: $C = 542$, $\mu_T = 150$, $\mu_R = 50$, $\sigma_R = 25$.

(c)

(d)

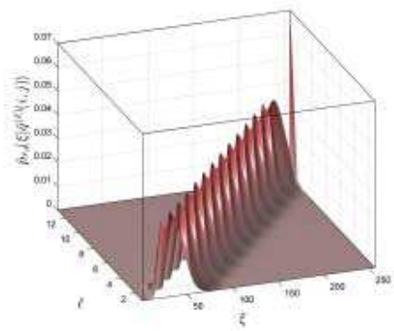

(e) The PDF for the blurring channel $\mathbf{A}_{\mathrm{BOM},\pi/4}$: $C = 612$, $\mu_T = 60$, $\mu_R = 40$, $\sigma_R = 35$.

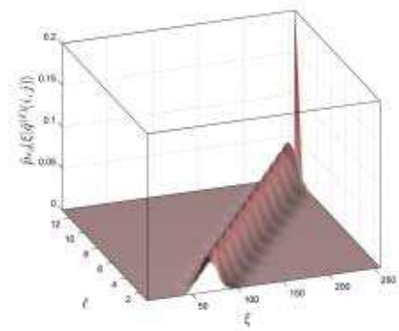

(f) The PDF for the blurring channel $\mathbf{A}_{\mathrm{BOM},\pi/4}$: $C = 542$, $\mu_T = 150$, $\mu_R = 50$, $\sigma_R = 25$.

(g)

(h)

Fig. 9. The examples of SODEM transfer (likeli-hood) functions with the corresponding realization $\mathbf{R}_d$ of the A/D converter output: $N_b = 8$, $\Delta_Q = 3$. All alphabets $\{q^{(\ell)}\}_{\ell=1}^{M_q}$ are sorted according to the size ($q^{(1)}$ is the least element and $q^{(M_q)}$ is the greatest element).

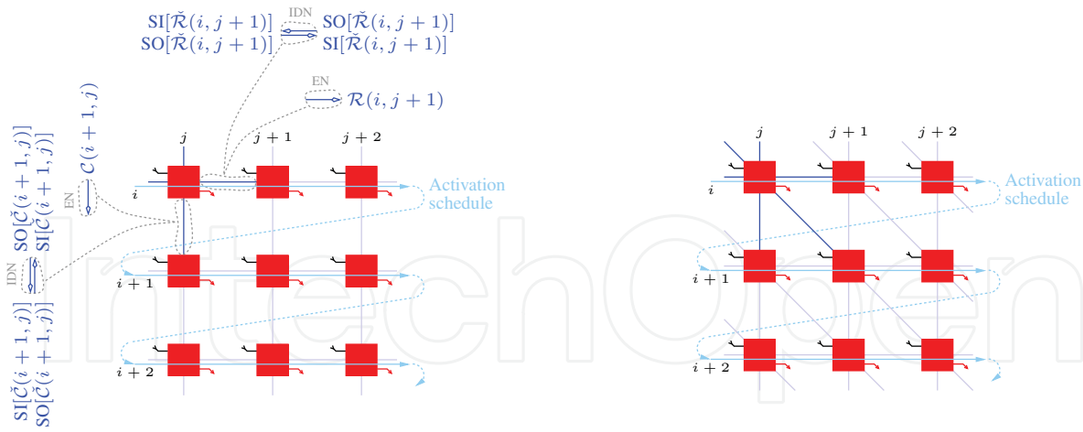

(a) The EN and IDN marginalizing at the symbol block level.

(b) The EN and IDN marginalizing at the symbol block level with bias state variables.

Fig. 10. The topology of the EN and IDN with denotation of the IDN activation schedule.

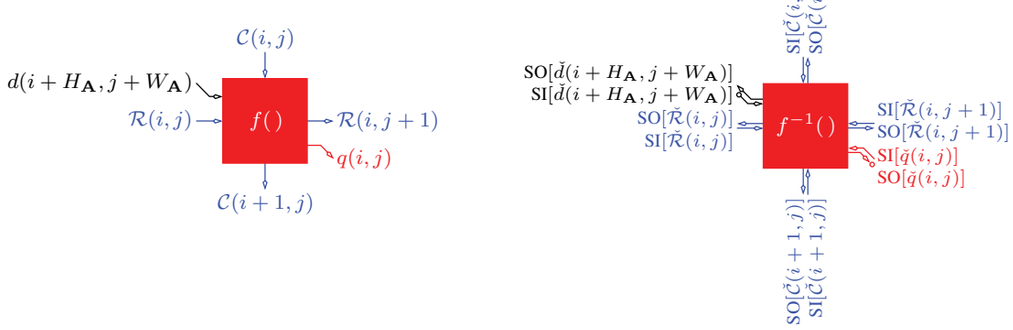

(a) The EN cell.

(b) The IDN cell (SISO module).

Fig. 11. The cells in the node (i, j) of the EN and IDN marginalizing at the symbol block level.

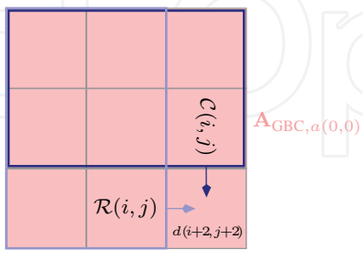

Fig. 12. The primary layout of auxiliary state variables $\mathcal{R}(i,j)$ and $\mathcal{C}(i,j)$ for the ISI channel $\mathbf{A}_{\mathrm{GBC},a(0,0)}$.

The quantities

$$\mathrm{SI}[\check{\mathcal{R}}(i,j)] = \underset{\check{d}(i,j)\in\check{\mathcal{R}}(i,j)}{\copyright} \mathrm{SI}[\check{d}(i,j)] \tag{30}$$

and

$$\mathrm{SI}[\check{\mathcal{C}}(i,j)] = \underset{\check{d}(i,j)\in\check{\mathcal{C}}(i,j)}{\copyright} \mathrm{SI}[\check{d}(i,j)], \tag{31}$$

before the first iteration of the IDN, are adjusted via combination of the a priori measures $\mathrm{SI}[\check{d}(i,j)]$ corresponding to testing estimators $\check{d}(i,j)$, that form block estimators $\check{\mathcal{R}}(i,j)$ and $\check{\mathcal{C}}(i,j)$.

7.2 Distributed IDN marginalizing at the symbol block level with bias state variables

The fundamental disadvantage of IDNs described in the previous paragraph rests in cardinality of state variables. For example decomposition in Fig. 12a has cardinality for dichromatic pictures 2^6 per variable and therefore both bidirectional concatenations of all SISO modules have to transfer $2 \times 2^6 = 128$ soft measures in the each direction. However, this is not only one disadvantage. The another rests in potential absence of the optimal decomposition for irregular kernels which can extremely gross up computational exigencies of the algorithm.

Impacts of both mentioned disadvantages can be reduced by the suggestion of EN structure in Fig. 10b that is expanded by the bias state variable $\mathcal{B}(i,j)$. All inputs and outputs of each node, shown in Fig. 13a, forms the set $\mathcal{N}_f(i,j) = \{\mathcal{R}(i,j), \mathcal{C}(i,j), \mathcal{B}(i,j), d(i+H_{\mathbf{A}}, j+W_{\mathbf{A}}), \mathcal{R}(i,j+1), \mathcal{C}(i+1,j), \mathcal{B}(i,j), q(i,j)\}$, where state variables are shaped by more liberal condition

$$\begin{aligned} \mathcal{N}_d(i,j) &\subseteqq \mathcal{R}(i,j) \cup \mathcal{C}(i,j) \cup \mathcal{B}(i,j) \cup d(i+H_{\mathbf{A}}, j+W_{\mathbf{A}}) \\ &\supset \mathcal{R}(i,j+1), \mathcal{C}(i+1,j), \mathcal{B}(i+1,j+1). \end{aligned} \tag{32}$$

In Fig. 12 are expressed three examples of decompositions for two different cores. Concretely, in the case of 1st version of kernel $\mathbf{A}_{\mathrm{GBC},a(0,0)}$ partitioning, where state variables are $\mathcal{R}(i,j) = \{d(i+1,j), d(i+1,j+1), d(i+2,j), d(i+2,j+1)\}$, $\mathcal{C}(i,j) = \{d(i,j+1), d(i,j+2), d(i+1,j+1), d(i+1,j+2)\}$ and $\mathcal{B}(i,j) = \{d(i,j), d(i+1,j), d(i,j+1), d(i+1,j+1)\}$, is necessary to transfer and store only $3 \times 2^4 = 48$ soft measures in the each direction. In the 2nd version for same kernel this number is smaller, namely $2 \times 2^3 + 2^2 = 20$.

The IDN topology copies the EN topology as in the previous case and activation schedule is identical too. A SISO module used in this IDN is approached in Fig. 13b.

7.3 Distributed IDN marginalizing at the symbol level

The topology of the IDN marginalizing at the symbol level is dependent on the shape of the response $\mathbf{A}$. It is the basic difference from the IDN marginalizing at the symbol block level, whose topology is invariable. There are two possible kinds of the topology. Either the topology centered on the response central coefficient or the shifted topology, that is fixed on the coefficient other than the central coefficient.

Firstly, we focus on the IDN example with the centered topology for the ISI channel $\mathbf{A}_{\mathrm{GBC},a(0,0)}$ with order $L = H_{\mathbf{A}} + 1 = W_{\mathbf{A}} + 1 = 3$. Let us suppose the source EN in Fig. 15a emulating the convolution

$$\begin{aligned} q(i,j) &= Cf(\mathbf{A}_{\mathrm{GBC},a(0,0)}, \mathcal{N}_d(i-1,j-1) \subset \mathbf{D}) \\ &= C \sum_{|i'|,|j'|\leq 1} a(i',j') d(i+i', j+j') \end{aligned} \tag{33}$$

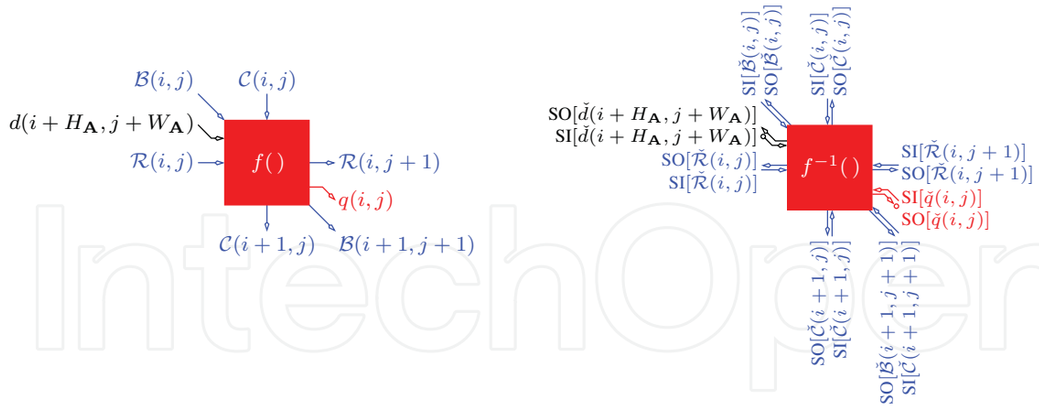

(a) The EN cell. (b) The IDN cell (SISO module).

Fig. 13. The cells in the node (i,j) of the EN and IDN marginalizing at the symbol block level with bias state variables.

Fig. 14. The two possible layouts of auxiliary state variables $\mathcal{R}(i,j)$, $\mathcal{C}(i,j)$ and $\mathcal{B}(i,j)$ for the ISI channel $\mathbf{A}_{\mathrm{GBC},a(0,0)}$.

centered on the central (dominant) coefficient $a(0,0)$. Each node (GPE) in this EN contains two functional blocks (broadcaster and combining element) with the generally variable system of inputs and outputs. In the our current example, each node has the framework shown in Fig. 15b and it is connected to the eight nearest neighbors. All these cells together creating the convolutional region $\mathcal{N}_d(i-1,j-1)$. An input and outputs of each broadcaster make the set

$$\mathcal{N}_B(i,j) = \{d(i,j), c(i,j,k) = d(i,j)\}_{1\le k\le 9}. \tag{34}$$

The outputs of nine neighboring broadcasters create inputs for one combining element. These inputs with the output

$$q(i,j) = C\sum_{0\le k\le 7} a(\lfloor 1/2+\sin(\pi k/4)\rfloor, \lfloor 1/2-\cos(\pi k/4)\rfloor)c(i+\lfloor 1/2+\sin(\pi k/4)\rfloor, j+\lfloor 1/2-\cos(\pi k/4)\rfloor, k+1) + Ca(0,0)c(i,j,9) \tag{35}$$

make the set

$$\mathcal{N}_f(i,j) = \{c(i+\lfloor 1/2+\sin(\pi k/4)\rfloor, j+\lfloor 1/2-\cos(\pi k/4)\rfloor, k+1), c(i,j,9), q(i,j)\}_{0\le k\le 7}. \tag{36}$$

As is known, the IDN has topology corresponding with the EN topology. One of the composite SISO modules creating the present IDN is illustrated in Fig. 15c, where the SISO module B^{-1} performing the combination

$$\mathrm{SO}[\check{d}(i,j)] = \underset{k}{\copyright}\mathrm{SI}[\check{c}(i,j,k) = \check{d}(i,j)] \tag{37}$$

with the marginalization

$$\mathrm{SO}[\check{c}(i,j,k)] = \left(\underset{k' \neq k}{\copyright}\ \mathrm{SI}[\check{c}(i,j,k') = \check{c}(i,j,k)]\right) \copyright \mathrm{SI}[\check{d}(i,j) = \check{c}(i,j,k)] \tag{38}$$

and the SISO module $f^{-1}()$ performing combination

$$\mathrm{S}[\check{\mathcal{N}}_f(i,j)] = \left(\underset{\check{c}(i',j',k) \in \check{\mathcal{N}}_f(i,j)}{\copyright} \mathrm{SI}[\check{c}(i',j',k)]\right) \copyright \mathrm{SI}[\check{q}(i,j)] \tag{39}$$

with the marginalizations

$$\mathrm{SO}[\check{c}(i',j',k)] = \left(\underset{\check{\mathcal{N}}_f(i,j):\check{c}(i',j',k)}{\text{Ⓜ}} \mathrm{S}[\check{\mathcal{N}}_f(i,j)]\right) \copyright^{-1} \mathrm{SI}[\check{c}(i',j',k)] \tag{40}$$

and $\mathrm{SO}[\check{q}(i,j)]$ acquisitionable from Eq. 29.

A soft measure processing in the composite SISO modules is mirrored to the signal processing in the EN nodes (from $d(i,j)$ to $q(i,j)$) and begins with activation all SISO modules $f^{-1}()$. Consequently, the activations of the SISO modules B^{-1} take place. Both activations, intimated by activation loops in Fig. 15a, form one iteration of the entire IDN. After finishing of all required iterations, the IDN makes hard decisions $\hat{d}(i,j)$ in accordance with Eq. 13.

The quantities $\mathrm{SI}[\check{c}(i,j,k)]$, before the first iteration of the IDN, are adjusted pursuant to the a priori measures $\mathrm{SI}[\check{d}(i,j)]$, because the $c(i,j,k)$ constitute copies of the $d(i,j)$. Henceforth, we come up to the IDN example again for the $\mathbf{A}_{\mathrm{GBC},3/10}$, but now it will be the IDN with the shifted topology. In this case, the source EN in Fig. 16a implements the convolution Eq. 1 centered on the upper left coefficient. One of the EN cells is shown in Fig. 16b. In comparison with the previous example, there is a difference only in the combining element. It has the I/O set

$$\mathcal{N}_f(i,j) = \{c(i - \lceil k/3 \rceil + 3, j + 3\lceil k/3 \rceil - k, k), q(i,j)\}_{1 \leq k \leq 9} \tag{41}$$

where

$$q(i,j) = C \sum_{1 \leq k \leq 9} a(i - \lceil k/3 \rceil + 3, j + 3\lceil k/3 \rceil - k) c(i - \lceil k/3 \rceil + 3, j + 3\lceil k/3 \rceil - k, k). \tag{42}$$

The soft inversion of the mentioned EN cell is represented by Fig. 16c and along with other cooperative SISO modules forming the resulting IDN. A similar IDN can be synthesized by the analogical way for any other ISI channel.

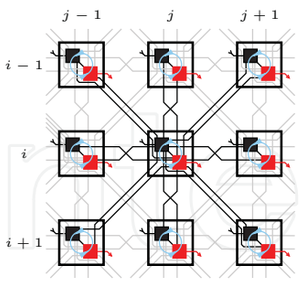

(a) The topology of the EN and IDN with denotation of the IDN activation schedule.

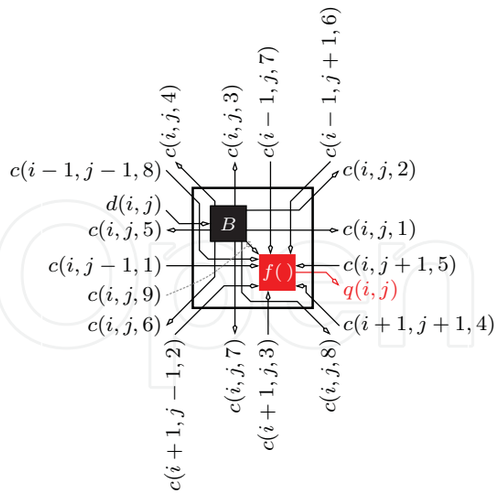

(b) The EN cell in the node (i,j). The connection of the broadcaster (■) and combining element (■).

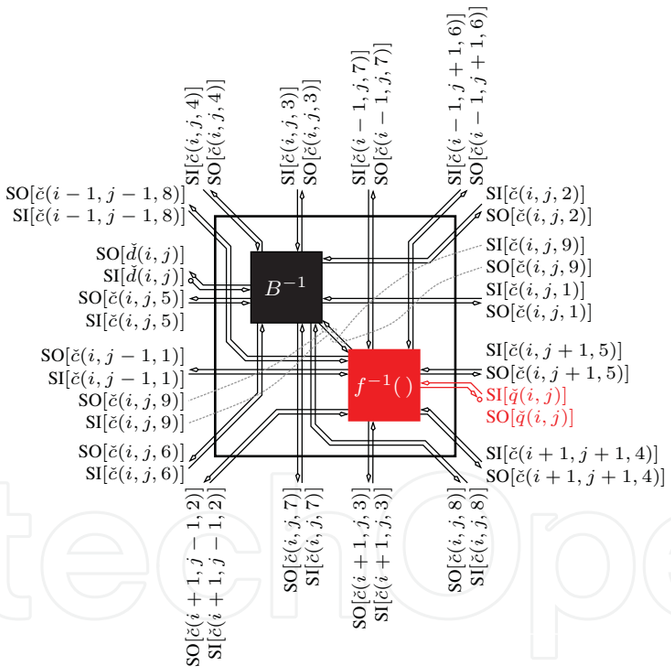

(c) The IDN cell (SISO module) in the node (i,j).

Fig. 15. The EN and IDN marginalizing at the symbol level with the centered topology for the ISI channel $\mathbf{A}_{\mathrm{GBC},a(0,0)}$.

7.4 Simplified distributed IDN marginalizing at the symbol level

If the response $\mathbf{A}$ has a dominant coefficient and the IDN topology is centered on this coefficient, then such IDN can be further numerically simplified by the approximation $\mathrm{SO}[\check{d}(i,j)] \approx \mathrm{SO}[\check{c}(i,j,\max(k))]$ (Chugg et al., 2001). It reduces a number of marginalizations

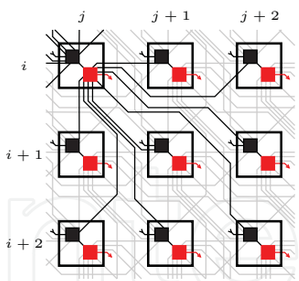

(a) The topology of the EN and IDN.

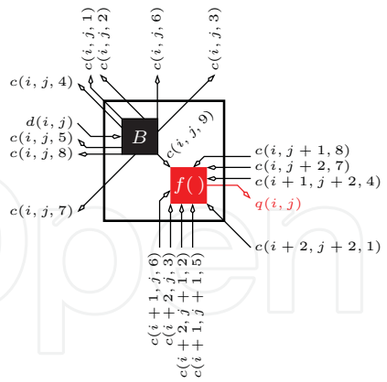

(b) The EN cell in the node (i, j).

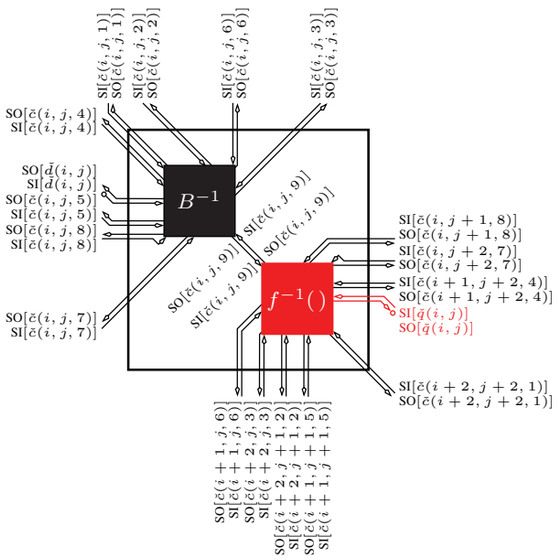

(c) The IDN cell in the node (i, j).

Fig. 16. The EN and IDN marginalizing at the symbol level with the shifted topology for ISI channel $\mathbf{A}_{\mathrm{GBC},a(0,0)}$.

in the SISO modules $f^{-1}()$ only to the variable $\check{c}(i, j, \max(k))$ and enables removing of all SISO modules B^{-1}.

Let us approach the principle of this approximation at the first IDN example in the paragraph 7.3. There had $\mathbf{A}$ the dominant coefficient $a(0,0)$. Therefore, the $\mathrm{SO}[\check{d}(i,j)]$ can be approximated by the $\mathrm{SO}[\check{c}(i,j,9)]$ and inputs $\{\mathrm{SI}[\check{c}(i + \lfloor 1/2 + \sin(\pi k/4) \rfloor, \; j + \lfloor 1/2 - \cos(\pi k/4) \rfloor, k + 1)]\}_{0 \le k \le 7}$ of associated SISO modules will be directly equal to $\mathrm{SO}[\check{c}(i,j,9)]$, as is shown in Fig. 17.

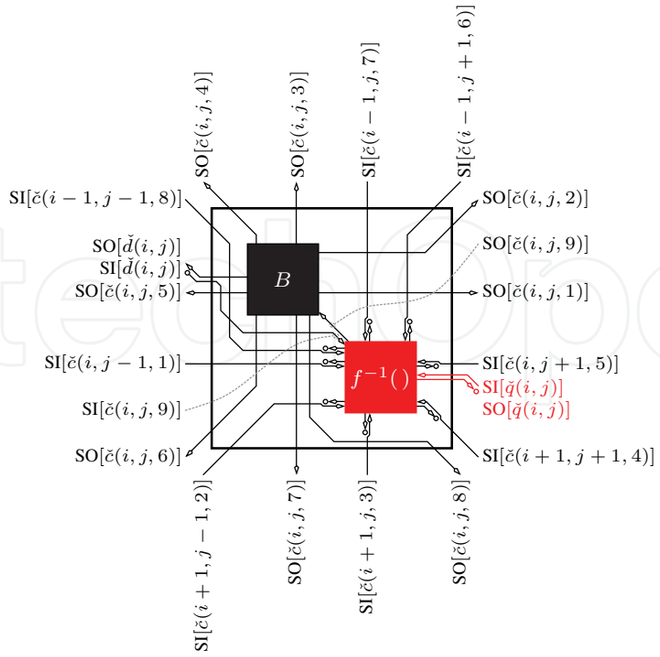

Fig. 17. The cell in the node (i,j) of the simplified IDN marginalizing at the symbol level with centered topology for the ISI channel $\mathbf{A}_{\mathrm{GBC},a(0,0)}$.

7.5 Layered IDN for an ISI channel with a decomposition-able impulse response

Finally, we focus on the Layered IDN for ISI channels with a decomposition-able impulse response to the horizontal $\mathbf{h} = [\,h'\ h\ h'\,]$ and vertical $\mathbf{g} = [\,g'\ g\ g'\,]$ direction. For example, the GBC has this property and therefore we assume, without detriment to generality, the GBC

$$\begin{aligned}\mathbf{A}_{\mathrm{GBC},gh} &= \mathbf{h}\mathbf{g}^T \\ &= \begin{bmatrix} h'g' & hg' & h'g' \\ h'g & hg & h'g \\ h'g' & hg' & h'g' \end{bmatrix}\end{aligned} \tag{43}$$

with size $L \times L = 3 \times 3$ that will be used for exemplary construction of the layered EN, shown in Fig. 18a, and mutually corresponding IDN, shown in Fig. 18b.

The signal processing (two-step convolution) starts on the EN bottom layer $c(i,j) = f_R(\mathbf{h}, \{d(i,j-2), d(i,j-1), d(i,j)\}) = h'd(i,j-2) + hd(i,j-1) + h'd(i,j)$ and continues on the EN top layer $\tilde{q}(i,j) = f_C(\mathbf{g}, \{c(i-2,j), c(i-1,j), c(i,j)\}) = g'c(i-2,j) + gc(i-1,j) + g'c(i,j))$. Each row-wise or column-wise concatenated node (GPE) creates a one functional block with the fixed system of inputs and outputs $\mathcal{N}_{f_R}(i,j) = \{\mathcal{R}(i,j), d(i,j), \mathcal{R}(i,j+1), c(i,j)\}$ or $\mathcal{N}_{f_C}(i,j) = \{\mathcal{C}(i,j), c(i,j), \mathcal{C}(i,j+1), q(i,j)\}$, where $\mathcal{R}(i,j) = \{d(i,j-2), d(i,j-1)\}$ and $\mathcal{C}(i,j) = \{c(i-2,j), c(i-1,j)\}$ present auxiliary state variables containing two symbols together, as in the case of the distributed IDN marginalizing at the symbol block level.

This specific case of the 2D ISI channel makes 2D detection, through the chosen EN topology, decomposition-able into double 1D detection, when in separate rows and columns can be used the well known Fixed interval forward-backward algorithm (FI FBA) Chugg et al. (2001). Let us elucidate the FI FBA principle on the IDN top layer. Its current recursion, in the node

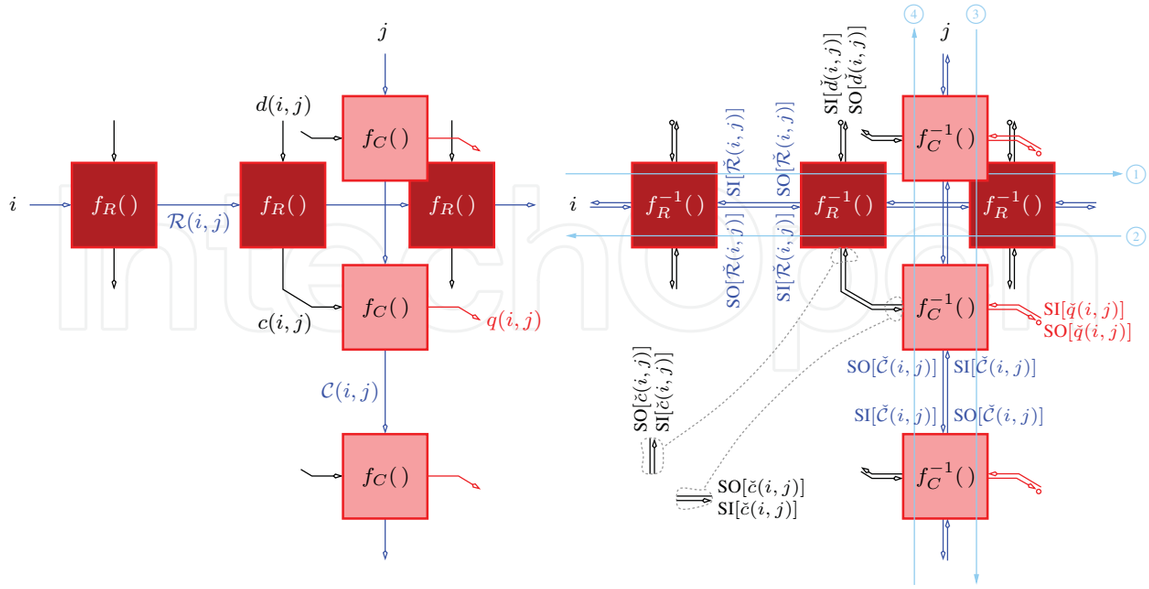

(a) The topology of the layered EN with illustration of individual EN cells.

(b) The topology of the layered IDN with illustration of individual IDN cells (SISO modules) and denotation of activation schedule.

Fig. 18. The layered EN and IDN for an ISI channel with a decomposition-able impulse response.

(i,j), is performed by following the sequence of operations: the combination (preprocessing — enumeration of auxiliary variables

$$\mathrm{S}[\check{\mathcal{N}}_{f_C}(i,j) \setminus \{\check{\mathcal{C}}(i,j), \check{\mathcal{C}}(i+1,j)\}] = \mathrm{S}[\check{c}(i,j)] \copyright \mathrm{SI}[\check{q}(i,j)] \tag{44}$$

and

$$\mathrm{S}[\check{\mathcal{N}}_{f_C}(i,j) \setminus \{\check{c}(i,j), \check{q}(i,j)\}] = \mathrm{S}[\check{\mathcal{C}}(i,j)] \copyright \mathrm{S}[\check{\mathcal{C}}(i+1,j)] \tag{45}$$

with their storage), the forward recursion ③ (top-down)

$$\mathrm{SO}[\check{\mathcal{C}}(i+1,j)] = \underset{\check{\mathcal{N}}_{f_C}(i,j):\check{\mathcal{C}}(i+1,j)}{\textcircled{M}} \mathrm{S}[\check{\mathcal{N}}_{f_C}(i,j) \setminus \{\check{\mathcal{C}}(i,j), \check{\mathcal{C}}(i+1,j)\}] \copyright \mathrm{SI}[\check{\mathcal{C}}(i,j)], \tag{46}$$

the backward recursion ④ (bottom-up)

$$\mathrm{SO}[\check{\mathcal{C}}(i,j)] = \underset{\check{\mathcal{N}}_{f_C}(i,j):\check{\mathcal{C}}(i,j)}{\textcircled{M}} \mathrm{S}[\check{\mathcal{N}}_{f_C}(i,j) \setminus \{\check{\mathcal{C}}(i,j), \check{\mathcal{C}}(i+1,j)\}] \copyright \mathrm{SI}[\check{\mathcal{C}}(i+1,j)] \tag{47}$$

and the completion operation (postprocessing — enumeration of output variables

$$\mathrm{SO}[\check{c}(i,j)] = \underset{\check{\mathcal{N}}_{f_C}(i,j):\check{c}(i,j)}{\textcircled{M}} \mathrm{S}[\check{\mathcal{N}}_{f_C}(i,j) \setminus \{\check{c}(i,j), \check{q}(i,j)\}] \copyright \mathrm{SI}[\check{q}(i,j)] \tag{48}$$

and

$$\mathrm{SO}[\check{q}(i,j)] = \underset{\check{\mathcal{N}}_{f_C}(i,j):\check{q}(i,j)}{\textcircled{M}} \mathrm{S}[\check{\mathcal{N}}_{f_C}(i,j) \setminus \{\check{c}(i,j), \check{q}(i,j)\}] \copyright \mathrm{SI}[\check{c}(i,j)] \quad \text{(optional)} \tag{49}$$

with their distribution to cooperative SISO modules). On the bottom layer is done identical process, directed by the rotated activation schedule merging the forward recursion ① and the backward recursion ②. The several iteration of the entire layered IDN creates firstly the FBA initiation on the top layer, terminated by the inter-marginalization $\{\mathrm{SO}[\check{c}(i,j)]\}_{i,j}$, and subsequently the same procedure on the bottom layer.

The hard decision $\hat{d}(i,j)$ and primary adjustment of the input soft measures $\mathrm{SI}[\check{\mathcal{R}}(i,j)]$ and $\mathrm{SI}[\check{\mathcal{C}}(i,j)]$ (before first iteration of the IDN) is similar as in the previous cases and they are directed by Eq. 13, Eq. 30 and Eq. 31.

7.6 Summary of IDNs properties

The introduced IDNs can be evaluated in four angles: computation exigences, implementation complexity, application flexibility and performance.

A distributed IDN marginalizing at the symbol level in comparison with the distributed IDN marginalizing at the symbol block level has less computation exigences and it is effectively applicable at whatever kind of the impulse response **A**. However it has plenty of jumpers on the other hand and its structure changes in accordance with the shape of the **A**. Each jumper presents one inside (auxiliary) variable, thus this IDN is highly suboptimal and with respect to marginalizations at the level of individual symbols (pixels) it fails on lower signal to noise ratios.

The structure of the distributed IDN marginalizing at the symbol block level is invariable for all responses **A**. Each SISO module always has the same inputs and outputs. Only shapes of the estimators $\check{\mathcal{R}}(i,j)$, $\check{\mathcal{C}}(i,j)$ and $\mathcal{B}(i,j)$ are various and for certain special responses **A** don't have to exist in the optimal form that leads to the computationally simplest IDN. Therefore this IDN can have considerably more exacting computational complexity than IDN marginalizing at the symbol level, but due to marginalizations at the level of symbol (pixel) blocks it offers a quality output, even as the signal to noise ratio is very low.

The advantage of the layered IDN for an ISI channels with a decomposition-able impulse responses rests in the inter-marginalization between both layers, that makes its computational complexity $\propto M_d^L + (M_d(2M_d-1)^{\frac{L-1}{2}})^L$ lower than complexity $\propto M_d^{L^2}$ of the both distributed IDNs. The worst properties has in the angle of application flexibility, because it can be applied only to some few ISI channels. In term of implementation complexity it is a structure relatively simple.

8. Implementation and complexity reduction issue

8.1 Tree-structured enumeration of combinations and marginalizations

We should use the tree-structured enumeration everywhere it is possible. It represents de facto a pipeline signal processing based upon an intermediate data usage. Fig. 19 shows this principle.

As the example using tree-structured implementation, let us expose the simple SISO module $f^{-1}()$ in Fig. 20, where $\check{\mathcal{N}}_f(i,j) = \{\check{c}(i,j-1,1), \check{c}(i,j,3), \check{c}(i,j+1,2), \check{q}(i,j)\}$. Such soft inversion is a component of the IDN marginalizing at the symbol level in Fig. 21.

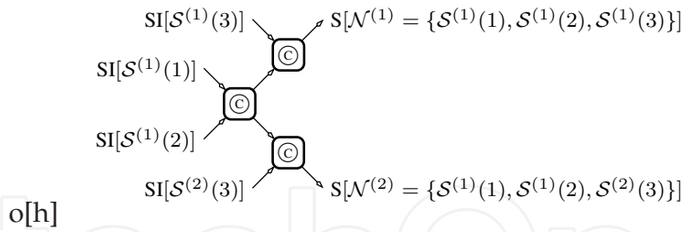

(a) Combinations.

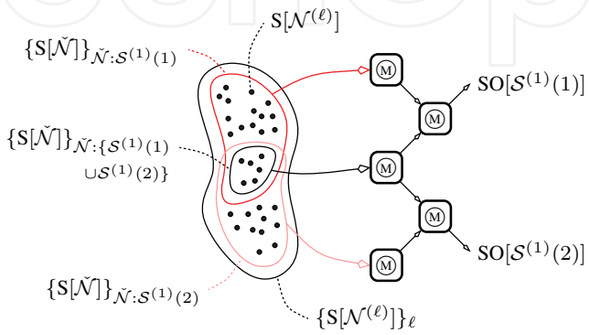

(b) Marginalizations.

Fig. 19. The tree-structured enumeration of combinations and marginalizations.

8.2 Fixation of the arithmetics

The most sensitive arithmetics have the IDNs implemented in the Pd. A large number of quantities less than 1 are multiplied in the SISO modules of such IDNs and the underflow of the arithmetics can happen. Therefore the Pd requires the regular scaling of the output measures

$$\mathrm{PO}[\mathcal{S}^{(\ell)}(k)] = \frac{\mathrm{PO}[\mathcal{S}^{(\ell)}(k)]}{\sum_\ell \mathrm{PO}[\mathcal{S}^{(\ell)}(k)]} \tag{50}$$

and so, the Md is preferable to a real implementation of the IDN. The arithmetics of the Md is relatively stable and can be protected from the incidental overflow by the scaling

$$\mathrm{MO}[\mathcal{S}^{(\ell)}(k)] = \mathrm{MO}[\mathcal{S}^{(\ell)}(k)] - \min_\ell \mathrm{MO}[\mathcal{S}^{(\ell)}(k)]. \tag{51}$$

But since the overflow is rare as the better scaling is $\mathrm{MO}[\mathcal{S}^{(\ell)}(k)] = \mathrm{MO}[\mathcal{S}^{(\ell)}(k)] - \mathrm{MO}[\mathcal{S}^{(1)}(k)]$ that allows discount the number of swapped measures by the fixed measure $\mathrm{MO}[\mathcal{S}^{(1)}(k)] = 0$.

8.3 Additional sub-optimality embedding complexity reduction

The distributed IDNs can be simplified in addition by the approximation neglecting least significant rays in the original response of the blurring channel. For example, the

$$\mathbf{A}_{\mathrm{GBC},0.2574} = \begin{bmatrix} 0.0607 & 0.1250 & 0.0607 \\ 0.1250 & 0.2574 & 0.1250 \\ 0.0607 & 0.1250 & 0.0607 \end{bmatrix}. \tag{52}$$

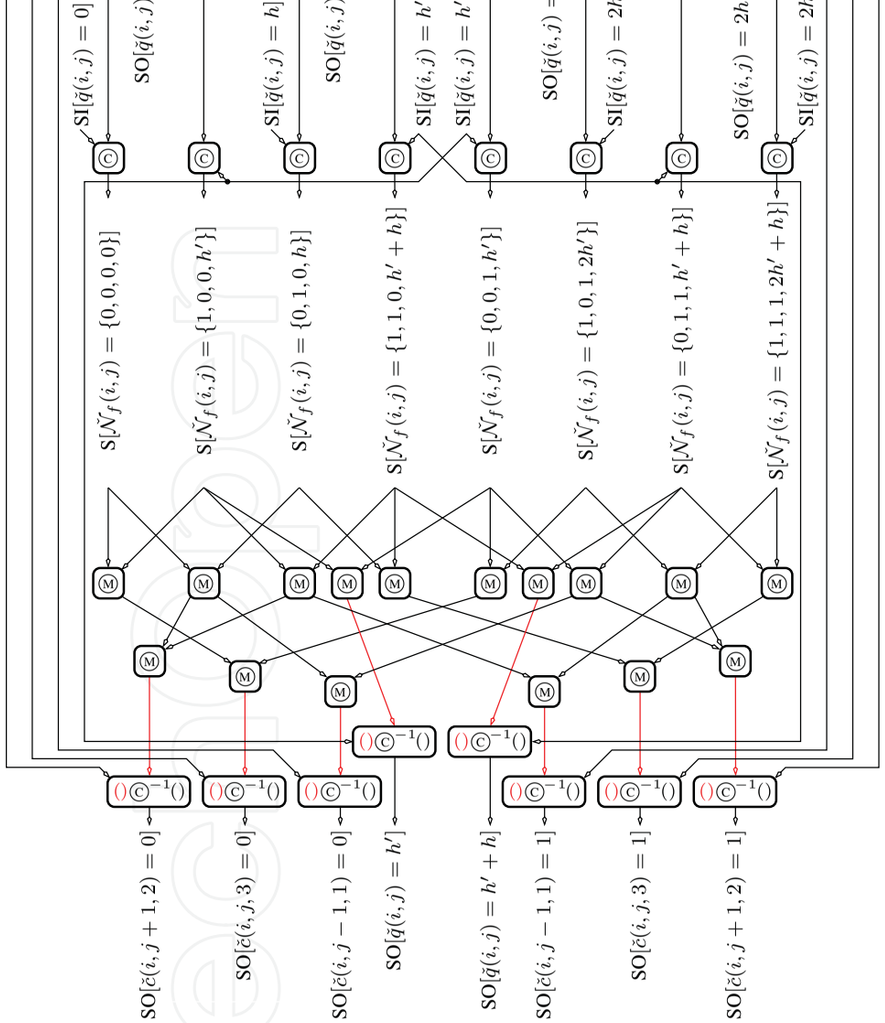

Fig. 20. The implementation of the SISO module $f^{-1}()$ using tree-structured enumeration of combinations and marginalizations, where $f()$: $q(i,j) = h'c(i,j-1,1) + hc(i,j,3)$ $+h'c(i,j+1,2)$

can be simplified to the form

$$\mathbf{A}_{\mathrm{SGBC},0.3399} = \begin{bmatrix} 0 & 0.1650 & 0 \\ 0.1650 & 0.3399 & 0.1650 \\ 0 & 0.1650 & 0 \end{bmatrix}. \tag{53}$$

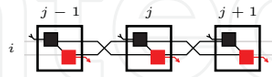

(a) The topology of the EN and IDN.

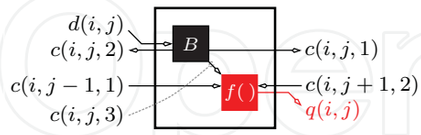

(b) The EN cell in the node (i, j).

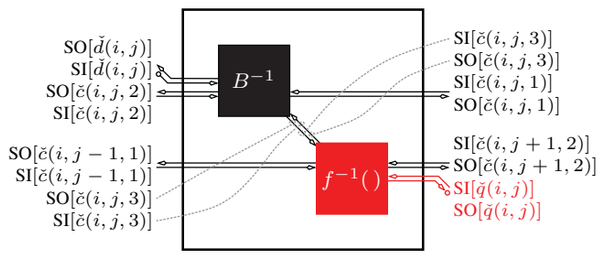

(c) The IDN cell in the node (i, j).

Fig. 21. The EN and IDN marginalizing at the symbol level with the centered topology for the horizontal ISI channel $\mathbf{A} = [\, h' \;\; h \;\; h' \,]$.

by the truncation of last four insignificant rays. The consequences of such approximation are illustrated in Fig. 23 and Fig. 22. In the both cases it reduces computational complexity to $\frac{1}{16}$. Moreover, it lowers the number of jumpers to one half in the case of the IDN marginalizing at the symbol level. The price paid for this rapid simplification rests in a quality degradation of the reconstructed picture.

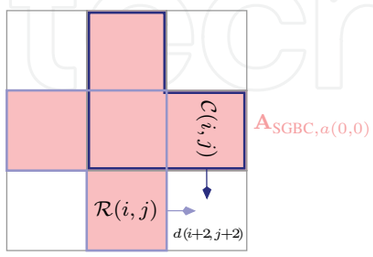

(a) Layouts for the IDN without bias state variable.

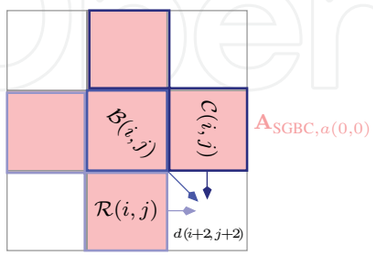

(b) Layouts for the IDN with bias state variable.

Fig. 22. The layouts of auxiliary state variables $\mathcal{R}(i, j)$, $\mathcal{C}(i, j)$ and $\mathcal{B}(i, j)$ in the IDN marginalizing at the symbol block level for the ISI channel $\mathbf{A}_{\mathrm{SGBC},a(0,0)}$.

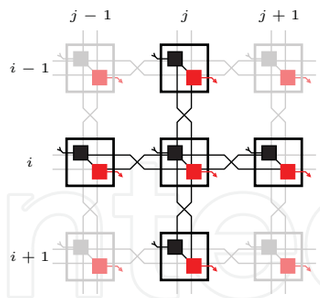

(a) The topology of the EN and IDN.

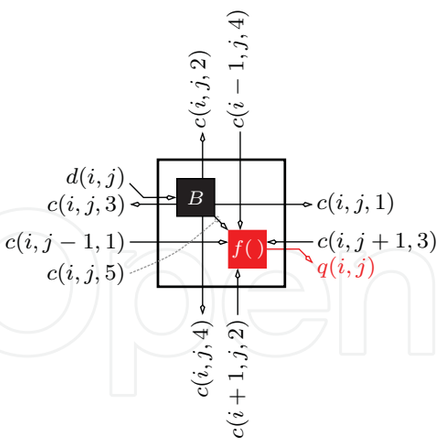

(b) The EN cell in the node (i,j).

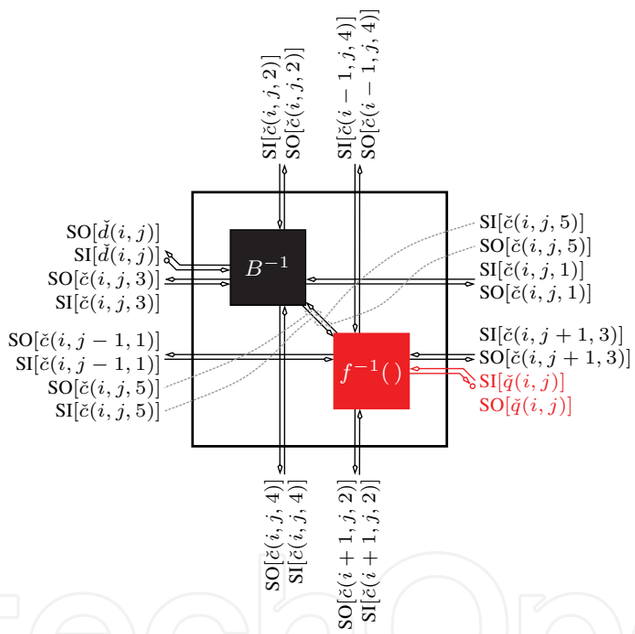

(c) The IDN cell in the node (i,j).

Fig. 23. The EN and IDN marginalizing at the symbol level with the centered topology for the ISI channel $\mathbf{A}_{\mathrm{SGBC},a(0,0)}$.

Can happen the situation, when the channel truncation causes the original 2D ISI channel atypical. Therefore, such kind of approximation is suitable especially for the IDN marginalizing at the symbol level, because it is a very flexible structure, applicable to the absolutely arbitrary 2D ISI channel. In case of the IDN marginalizing at the symbol block level can occur the problem with fulfillment of the condition $\mathcal{N}_d(i,j) = \mathcal{R}(i,j) \cup \mathcal{C}(i,j) \cup d(i + H_{\mathbf{A}}, j + W_{\mathbf{A}})$ and the estimators $\check{\mathcal{R}}(i,j)$ and $\check{\mathcal{C}}(i,j)$ don't have to exist in the optimal shapes that lead to the computationally simplest IDN.

9. Examples of dichromaric picture restoration, performance analyses and conclusions

9.1 Suppression of the defocusing in the imperfectly adjusted lens (GBC) with BER performance analyses

We will demonstrate the IDNs functionality on QR code snapshot restorations by the IDNs marginalizing at the symbol block level that were described in paragraphs 7.1 and 7.2. In Fig. 24 and Fig. 25 are shown example restorations of two different QR codes by the 1st and 2nd version of IDNs with bias state variables. Additionally, all versions of these IDNs has been tested with the Monte Carlo method for performance and compared with simple threshold detector, based on the relation $\hat{d}_{TD}(i,j) = \arg\min_{\check{d}(i,j)\in\{0,1\}} |\frac{x_d(i,j)-\hat{\mu}_T}{C} - \check{d}(i,j)|$. The result of this analysis is the set of BER curves shown in Fig. 26 and Fig. 27. As we can see in the BER curves, all tested IDNs have almost same performance and especially in the area of higher defocusing the usage is expedient. However, the performance slightly falls down in the focusation rising and at the beginning of iterative process. It is caused by diminishing corelation among individual neighboring pixels when iteratively precised state variables do not carry so fundamental and strong information worth to the current node of the network.

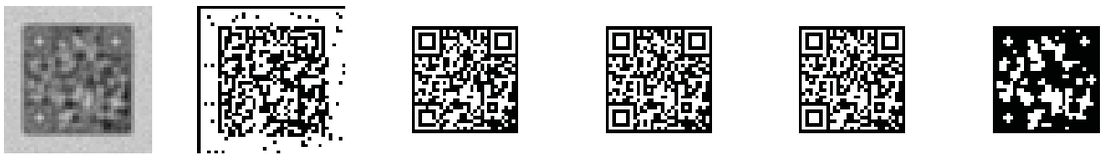

$\mathbf{R}_d$ | $\hat{\mathbf{D}}$, $I = 1$, BER $= 0.208$ | $\hat{\mathbf{D}}$, $I = 3$, BER $= 0.033$ | $\hat{\mathbf{D}}$, $I = 5$, BER $= 0.022$ | $\hat{\mathbf{D}}$, $I = 7$, BER $= 0.018$ | $\hat{\mathbf{D}}_{TD}$, BER $= 0.141$

Fig. 24. The example of the QR code restoration by the distributed IDN marginalizing at the symbol block level with bias state variables (Pd-SyD, 1st version): Kernel $\mathbf{A}_{\mathrm{GBC},2/10}$, $N_b = 8$, $\Delta_Q = 3$, $C = 612$, $\mu_T = 50$, $\mu_R = 25$, $\sigma_R = 10$.

$\mathbf{R}_d$ | $\hat{\mathbf{D}}$, $I = 1$, BER $= 0.168$ | $\hat{\mathbf{D}}$, $I = 3$, BER $= 0.021$ | $\hat{\mathbf{D}}$, $I = 5$, BER $= 0.006$ | $\hat{\mathbf{D}}$, $I = 7$, BER $= 0.004$ | $\hat{\mathbf{D}}_{TD}$, BER $= 0.085$

Fig. 25. The example of the QR code restoration by the distributed IDN marginalizing at the symbol block level with bias state variables (Pd-SyD, 2nd version): Kernel $\mathbf{A}_{\mathrm{GBC},2/10}$, $N_b = 8$, $\Delta_Q = 3$, $C = 612$, $\mu_T = 50$, $\mu_R = 25$, $\sigma_R = 10$.

In other words, the output $\{\mathrm{SI}[d^{(\ell)}(i + H_{\mathbf{A}}, j + W_{\mathbf{A}})]\}_\ell$ of current node strongly depends only on the input $\{\mathrm{SI}[q^{(\ell)}(i,j)]\}_\ell$ (product of the SODEM) and not so much on the state information $\{\mathrm{SI}[\mathcal{R}^{(\ell)}(i,j)]\}_\ell$, $\{\mathrm{SI}[\mathcal{R}^{(\ell)}(i,j+1)]\}_\ell$, $\{\mathrm{SI}[\mathcal{C}^{(\ell)}(i,j)]\}_\ell$, $\{\mathrm{SI}[\mathcal{C}^{(\ell)}(i+1,j)]\}_\ell$, $\{\mathrm{SI}[\mathcal{B}^{(\ell)}(i,j)]\}_\ell$ and $\{\mathrm{SI}[\mathcal{B}^{(\ell)}(i+1,j+1)]\}_\ell$ from other nodes as in the case of high defocusing.

Mentioned BER curves leads to conclusion, that the application of IDNs with bias state variables is better than standard IDNs marginalizing at the symbol block level, because bring evident implementation advantages beside performance preservation. In the case of 1st version it is consensus in the output state variables $\mathcal{R}(i,j+1) = \mathcal{C}(i+1,j) = \mathcal{B}(i+1,j+1)$, that warrants equation $\mathrm{SI}[\check{\mathcal{R}}(i,j+1)]©\mathrm{SI}[\check{\mathcal{R}}(i,j+1)] = \mathrm{SI}[\check{\mathcal{C}}(i+1,j)]©\mathrm{SI}[\check{\mathcal{C}}(i+1,j)] = \mathrm{SI}[\check{\mathcal{B}}(i+1,j+1)]©\mathrm{SI}[\check{\mathcal{B}}(i+1,j+1)]$ and allows only one and same marginalization for whole triplet of the state variables. On the other hand, the 2nd version is visible significant reduction of state variable cardinalities.

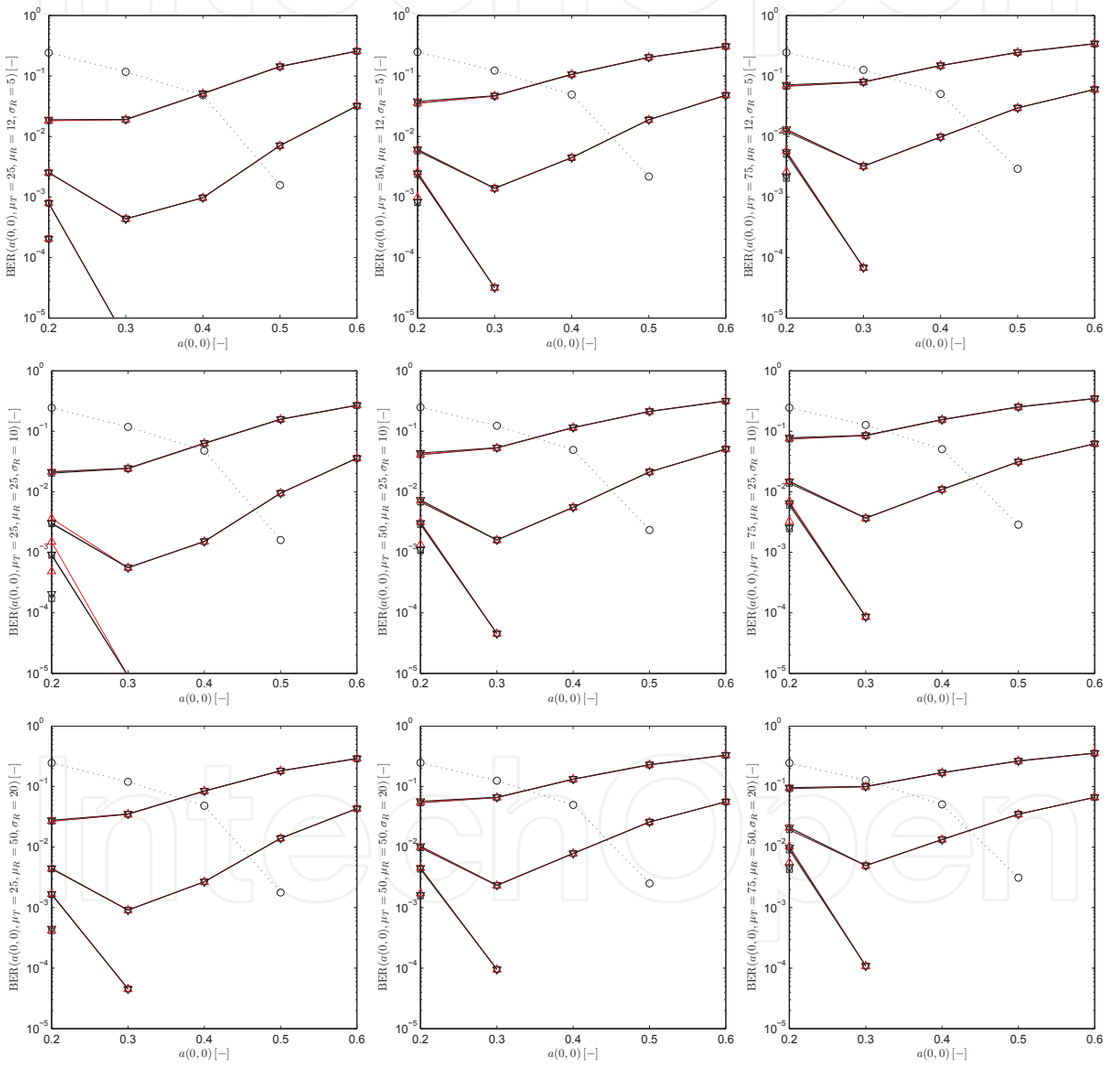

Fig. 26. The BER curves (1st, 2nd, 3th and 7th iteration) of the distributed IDN marginalizing at the symbol block level (Pd-SyD, black line with squares) and distributed IDN marginalizing at the symbol block level with bias state variables (Pd-SyD, 1st version — red line with triangles, 2nd version — black line with triangles): Kernel $\mathbf{A}_{\mathrm{GBC},a(0,0)}$, $N_b = 8$, $\Delta_Q = 3$, $C = 612$. The comparison with BER curves (dot line with circles) of the threshold detector.

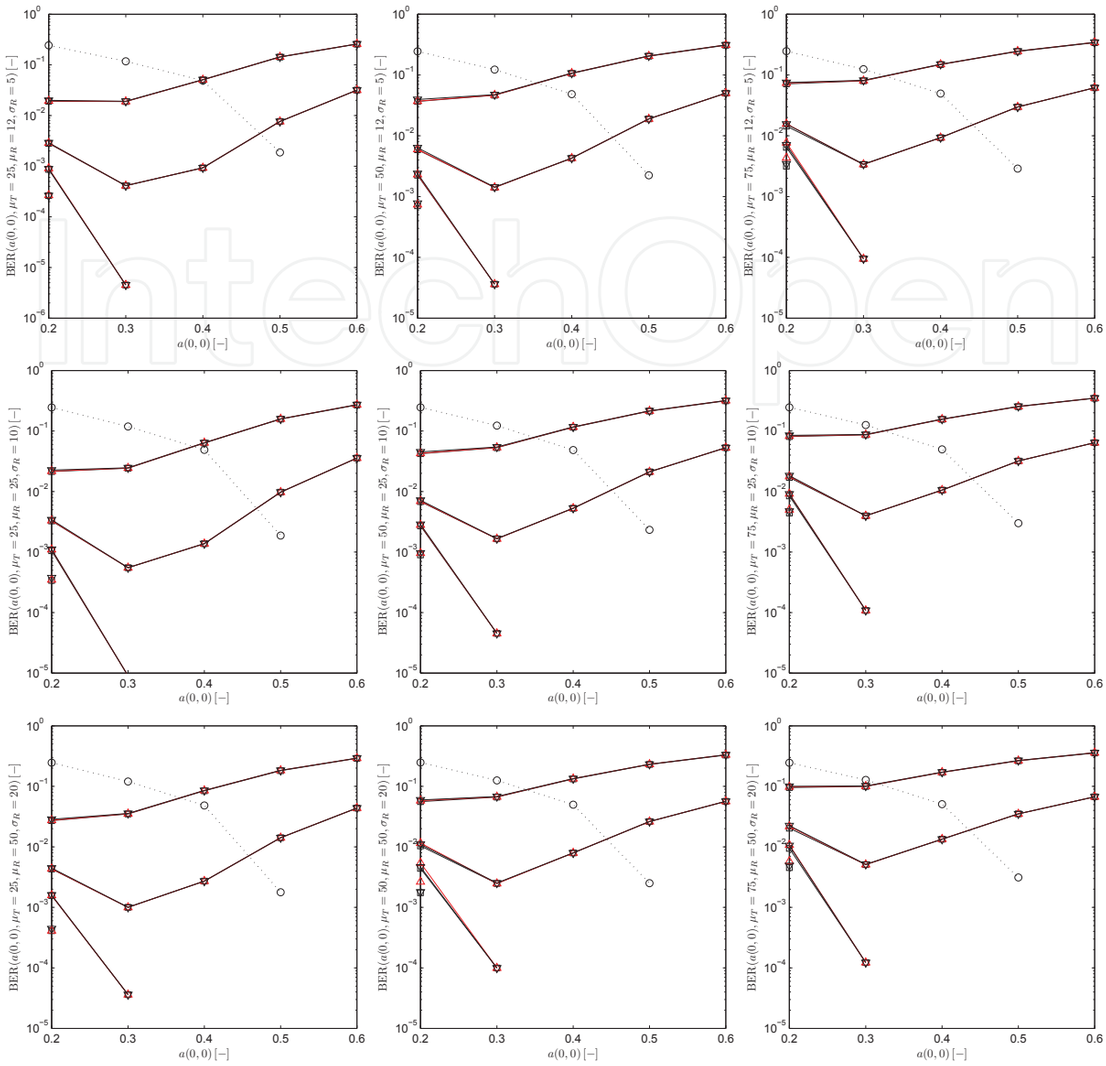

Fig. 27. The BER curves (1st, 2nd, 3th and 7th iteration) of the distributed IDN marginalizing at the symbol block level (Pd-PgD, black line with squares) and distributed IDN marginalizing at the symbol block level with bias state variables (Pd-PgD, 1st version — red line with triangles, 2nd version — black line with triangles): Kernel $\mathbf{A}_{\mathrm{GBC},a(0,0)}$, $N_b = 8$, $\Delta_Q = 3$, $C = 612$. The comparison with BER curves (dot line with circles) of the threshold detector.

9.2 Suppression of the blurring due to object moving (BOM)

In this case we use for functionality demonstration the IDNs marginalizing at the symbol level. The following Fig. 31 shows the sample pictures restored by these IDNs for two different combination of the BOM. Used IDNs (theirs topologies) are represented in Fig 29 and Fig 30. Of course the IDNs marginalizing at the symbol block level can be used for this issue too. Theirs state variables are shown in Fig. 28.

The usage without whatever other supporting aids (external synchronization) demands the perfect knowledge about the scanned moving object ($\mathbf{s}_S$ and velocity vector). But, if all

mentioned conditions are fulfilled, the IDN produces a high quality output (estimation $\hat{\mathbf{D}}$) on the other hand.

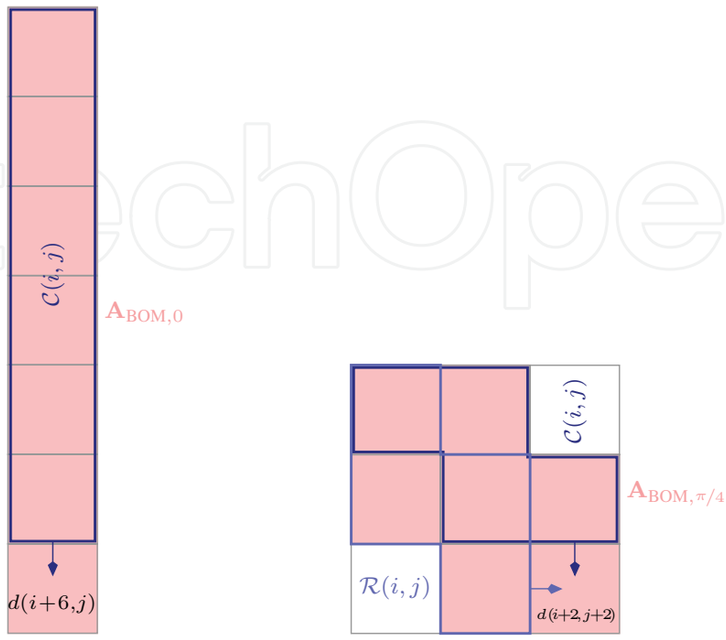

(a) $\mathbf{A}_{\mathrm{BOM},0}$. (b) $\mathbf{A}_{\mathrm{BOM},\pi/4}$.

Fig. 28. The shapes of auxiliary state variables $\mathcal{R}(i,j)$ and $\mathcal{C}(i,j)$ in the IDN marginalizing at the symbol block level for the ISI channel $\mathbf{A}_{\mathrm{BOM},\varphi}$.

The example of the IDN malfunction, caused by the wrong movement parameters adjustment, is demonstrated in Fig. 32. Suppose that the true starting point is $\mathbf{s}'_s$ and corresponds with the correct impulse response

$$\mathbf{A}'_{\mathrm{BOM},0} = \begin{bmatrix} \frac{1}{24} & \frac{1}{12} & \frac{1}{12} & \frac{1}{12} & \frac{1}{12} & \frac{1}{24} \\ \\ \frac{1}{24} & \frac{1}{12} & \frac{1}{12} & \frac{1}{12} & \frac{1}{12} & \frac{1}{24} \end{bmatrix}^T, \tag{54}$$

This response makes the blurring in Fig. 32b. If the IDN is consequently fed by the wrong impulse response $\mathbf{A}_0$ coming from the shifted point $\mathbf{s}_s$, then its failure, shown in Fig. 32c, is going to happen. It presents a serious problem, because we mostly have not available so accurate information about the movement of the scanned object. Thus, in the overwhelming majority of real applications, the IDN will have been supplemented by the auxiliary synchronizer performing the reliable estimation $\hat{\mathbf{s}}'_s$ of the $\mathbf{s}'_s$ placement inside the blue square in Fig. 32a.

The section vehicle speed measurement appears to be the most suitable application of the described method, because it is based on the signplate detection at the beginning and at the end of the monitored section, where the scanned vehicles have the same direction of the movement. So, the synchronization of the IDN will not represent a serious issue in this application.

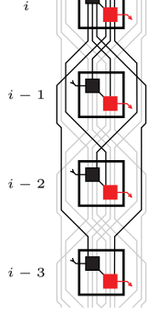

(a) The topology of the EN and IDN.

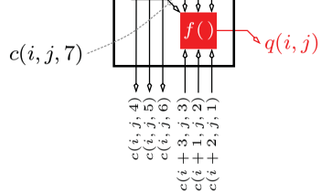

(b) The EN cell in the node (i,j).

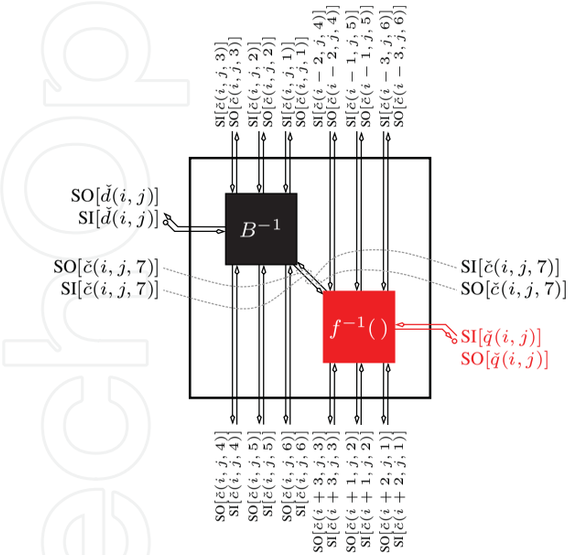

(c) The IDN cell in the node (i,j).

Fig. 29. The EN and IDN marginalizing at the symbol level with the centered topology for the ISI channel $\mathbf{A}_{\mathrm{BOM},0}$.

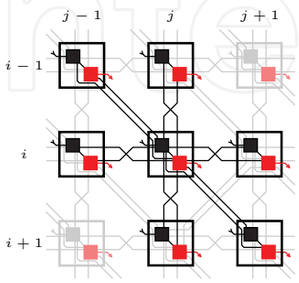

(a) The topology of the EN and IDN.

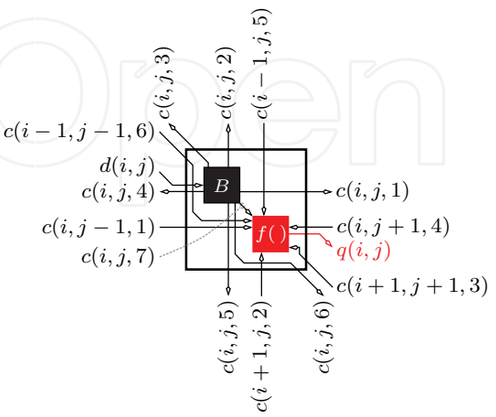

(b) The EN cell in the node (i,j).

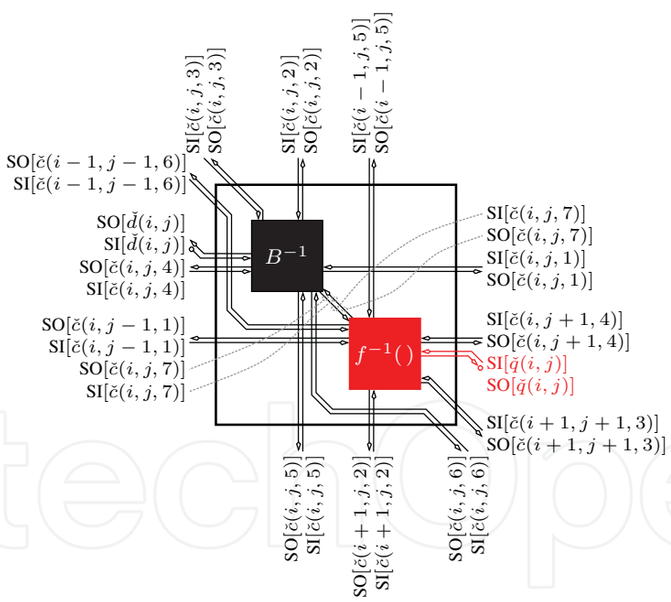

(c) The IDN cell in the node (i,j).

Fig. 30. The EN and IDN marginalizing at the symbol level with the centered topology for the ISI channel $\mathbf{A}_{\mathrm{BOM},\pi/4}$.

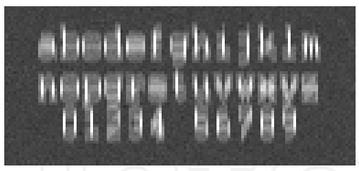

(a.1) The realization $\mathbf{R}_d$ of the A/D converter output.

(a.2) The hard decision $\hat{\mathbf{D}}$ after 3^{th} iteration of the IDN.

(a.3) The hard decision $\hat{\mathbf{D}}$ after 7^{th} iteration of the IDN.

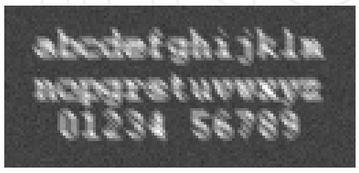

(b.1) The realization $\mathbf{R}_d$ of the A/D converter output.

(b.2) The hard decision $\hat{\mathbf{D}}$ after 3^{th} iteration of the IDN.

(b.3) The hard decision $\hat{\mathbf{D}}$ after 7^{th} iteration of the IDN.

Fig. 31. The examples of image restorations by the distributed IDN marginalizing at the symbol level (Pd-PgD) for the channels $\mathbf{A}_{\text{BOM},0}$(a) and $\mathbf{A}_{\text{BOM},\pi/4}$(b) merged with the simple noise model including the thermal noise and the quantization noise: $N_b = 8$, $\Delta_Q = 3$, $C = 768$, $\mu_T = 200$.

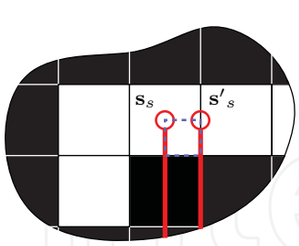

(a) The trajectory starting point displacement.

(b) The realization $\mathbf{R}_d$ of the A/D converter output.

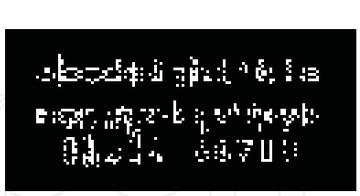

(c) The hard decision $\hat{\mathbf{D}}$ after 7^{th} iteration of the wrong adjusted IDN.

Fig. 32. The example of the wrong image restoration by the distributed IDN marginalizing at the symbol level (Pd-PgD), that was incorrectly set by the $\mathbf{A}_{\text{BOM},0}$ at the true blurring $\mathbf{A}'_{\text{BOM},0}$ merged with the simple noise model including the thermal noise and the quantization noise: $C = 768$, $N_b = 8$, $\Delta_d = 3$, $\mu_T = 200$.

9.3 Conclusions and open problems

The IDNs are based on the optimal (the best) MAP detector and so they are mostly able to obtain the optimal estimation. The IDN, analogous to the optimal detector, forms all possible variants of the input image and compares them with the corrupted image by the decision metric perfectly matched to the noise distribution. There is the difference only in fact, that the IDN solves this issue smartly by the suitable image segmentation and with minimal computational exigencies. This can be considered as the greatest advantage of the IDNs.

The important disadvantage rests in the application limitations, because the contemporary IDNs are able to restore a dichromatic (or black and white) patterns only (texts, car sign plates, QR codes, etc.). For restoration of grayscale or color image restorations and larger 2D ISI channels, where the number of all possible realizations of current convolution region $\{\mathcal{N}^{(\ell)}\}_\ell$ extremely grows, the IDN will require the another sub-optimality embedding simplification (generalization). Although the IDNs perform the segmental image processing, the numerical complexity is extreme. Individual SISO modules in the IDN can not be implemented directly as was shown on the simple example in Fig. 20, but must be realized also as the certain iterative system. This would establish an iterative detection network where each inner cell presents iterative subnet. The question remains how a single-shot SISO can be approximated to the iterative subnet. If it is possible and what level of sub-optimality this establish and whether this sub-optimality allows the good and fast convergence of the entire system to the correct solution. At present it is only surmise without concrete and functional results. But it is clear, that such network will be more suboptimal and its performace will not be so good as in the case of black & white images, where SISO module can be implemented as a single-shot (optimal) system. The next problem rests in fact, that is not possible analytically predicate the behaviour of such network due to extreme quantity of functional blocks and interconnections. Therefore the computer simulation and debuging will be very difficult and based on the labour principle. However, this method has very good application in the case of black & white images and it is completely different from classical methods like adaptive filtration, minimum mean square errors, etc. Because it is perfectly matched to the noise distribution and reconstruct image from all possible images by the intelligent way. Thanks to this ability the IDN is very powerful and can find good use in the area of image halftoning (Chugg et al., 2001), text detection, QR code detection, number plate detection of cars (traffic monitoring system), etc.

The last problem rests in the iterative detection network synchronization. In all cases it was considered that the IDN has perfect knowledge about kernel of the 2D ISI channel. This information, however, in reality it is not known and must be estimated. A Soft decision directed (SDD) Channel state estimator (CSE) can be used for this purposes. One of the most suitable CSEs for an IDN synchronization is the Expectation-Maximization (EM) algorithm. Its greatest benefit rests in the implementation simplicity and additional information about the algorithm can be found in (Noels et al., 2003).

10. References

Chugg, K.; Anastasopoulos, A. & Chen, X. (2001). *Iterative detection : Adaptivity, Complexity reduction and Applications*, Kluwer Academic Publishers, ISBN 0-470-84757-3.

Vucetic, B. & Juan, J. (2003). *Space-Time coding*, Kluwer Academic Publishers, ISBN 0-470-84757-3.

Vucetic, B. & Juan, J. (2000). *Turbo codes : Principles and Applications*, Kluwer Academic Publishers, ISBN 0-792-37868-7.

Kekrt, D. & Klíma, M. (2008). A black & white picture reconstruction by iterative detection network in the image capturing system with CCD (CMOS) sensor, *50th International Symposium ELMAR-2008*, Vol. 1, pp. 125-128, ISBN 978-953-7044-06-0, Zadar, Croatia, September 2008.

Kekrt, D. & Klíma, M. (2008). The iterative detection network based recovery of black & white pictures shot by camera — implementation and complexity reduction issue, *In Proceedings of the 18th International Conference Radioelektronika 2008*, pp. 219-222, ISBN 978-1-4244-2087-2, Prague, Czech Republic, April 2008.

Kekrt, D. & Klíma, M. (2008). Layered Iterative detection network based text recognition in the snapshot gained by camera with CCD (CMOS) sensor, *In Proceedings of the 12th International Student Conference on Electrical Engineering POSTER 2008* [CD-ROM], Prague, Czech Republic, May 2008.

Kekrt, D.; Klíma, M. & Podgorny, R. (2008). The iterative detection network suppression of defocusing and thermal noise in black and white pictures shot by a camera with CCD/CMOS sensor, *6th International Conference on Photonics, Devices and Systems*, Vol. 7138, pp. 71381Z-1-71381Z-7, ISBN 978-0-8194-7379-0, Prague, Czech Republic, August 2008.

Kekrt, D.; Klíma, M. & Fliegel, K. (2008). The iterative detection network based suppression of the thermal noise and blurring due to object moving in black and white pictures shot by a camera with CCD/CMOS sensor, *In Proceedings of SPIE Optics + Photonics*, Vol. 7076, pp. 70760M-1-70760M-9, ISBN 978-0-8194-7296-0, San Diego, USA, August 2008.

Kekrt, D.; Klíma, M. & Podgorny, R. (2008). Aspects of Image Quality Enhancement in Security Technology, *IEEE International Carnahan Conference on Security Technology 2008*, pp. 142-149, ISBN 978-1-4244-1816-9, Prague - Czech Republic, October 2008.

Kekrt, D. & Klíma, M. (2008). The advanced noise model for an IDN based restoration of black and white pictures captured by a camera with CCD/CMOS sensor, *IEEE International Carnahan Conference on Security Technology 2008*, pp. 126-130, ISBN 978-1-4244-1816-9, Prague, Czech Republic, October 2008.

J. van Vliet L.; Boddeke F. R.; Sudar D. & Young I.T. (1998). Image detectors for digital image microscopy. *M.H.F. Wilkinson, F. Schut (eds.), Digital Image Analysis of Microbes; Imaging, Morphometry, Fluorometry and Motility Techniques and Applications, Modern Microbiological Methods*, pp. 37-64, John Wiley & Sons, Chichester, The United Kingdom, 1998.

Anastasopoulos, A. & Chugg, K. (2000). Adaptive soft-input soft-output algorithms for iterative detection with parametric uncertainty. *IEEE Trans. Commun.*, Vol. 48, pp. 1638-1649, Oct. 2000.

Noels, N.; Herzet, C.; Dejonghe, A.; Lottici, V. ; Steendam, H.; Moeneclaey, M.; Luise, M.; Vandendorpe, L. (2003). Turbo synchronization : an EM algorithm interpretation, *IEEE International Conference on Communications - ICC*, 2003.

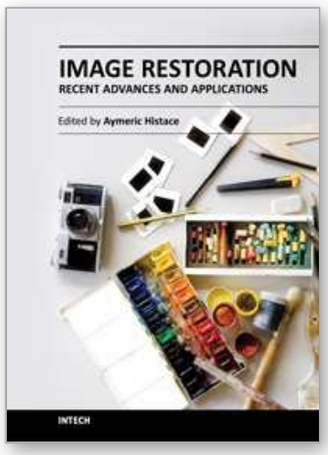

Image Restoration - Recent Advances and Applications

Edited by Dr Aymeric Histace

ISBN 978-953-51-0388-2
Hard cover, 372 pages
Publisher InTech
Published online 04, April, 2012
Published in print edition April, 2012

This book represents a sample of recent contributions of researchers all around the world in the field of image restoration. The book consists of 15 chapters organized in three main sections (Theory, Applications, Interdisciplinarity). Topics cover some different aspects of the theory of image restoration, but this book is also an occasion to highlight some new topics of research related to the emergence of some original imaging devices. From this arise some real challenging problems related to image reconstruction/restoration that open the way to some new fundamental scientific questions closely related with the world we interact with.

How to reference

In order to correctly reference this scholarly work, feel free to copy and paste the following:

Daniel Kekrt and Miloš Klima (2012). 2D Iterative Detection Network Based Image Restoration: Principles, Applications and Performance Analysis, Image Restoration - Recent Advances and Applications, Dr Aymeric Histace (Ed.), ISBN: 978-953-51-0388-2, InTech, Available from: http://www.intechopen.com/books/image-restoration-recent-advances-and-applications/2d-iterative-detection-network-based-image-restoration

INTECH
open science | open minds

InTech Europe
University Campus STeP Ri
Slavka Krautzeka 83/A
51000 Rijeka, Croatia
Phone: +385 (51) 770 447
Fax: +385 (51) 686 166
www.intechopen.com

InTech China
Unit 405, Office Block, Hotel Equatorial Shanghai
No.65, Yan An Road (West), Shanghai, 200040, China
中国上海市延安西路65号上海国际贵都大饭店办公楼405单元
Phone: +86-21-62489820
Fax: +86-21-62489821

IntechOpen